To the Graduate Council:

I am submitting herewith a thesis written by Carol P. Fryer entitled "The Effect of One-Half and One Atomic Percent Additions of Iron, Aluminum, Silicon, and Chromium on the Ordering Reaction of Ni_4Mo." I recommend that it be accepted in partial fulfillment of the requirements for the degree of Master of Science, with a major in Metallurgical Engineering.

J. E. Spruiell, Major Professor

We have read this thesis
and recommend its acceptance:

E. E. Hansbury

C R Brooks

Accepted for the Council:

L Evans Beth
Vice Chancellor
Graduate Studies and Research

THE EFFECT OF ONE-HALF AND ONE ATOMIC PERCENT ADDITIONS OF IRON, ALUMINUM, SILICON, AND CHROMIUM ON THE ORDERING REACTION OF Ni_4Mo

A Thesis

Presented for the

Master of Science

Degree

The University of Tennessee, Knoxville

Carol P. Fryer

March 1982

3057959

ACKNOWLEDGMENTS

The author wishes to thank Dr. J. E. Spruiell and Dr. E. E. Stansbury for their guidance and aid throughout this research. Appreciation is also extended to Dr. C. R. Brooks and Dr. B. F. Oliver for their technical assistance and to Dr. Brooks for serving on the thesis committee.

ABSTRACT

This thesis is a continuation of research done in recent years at the University of Tennessee concerning the nature of the order-disorder reaction in the alloy Ni_4Mo. The effect of 0.5 and 1.0 atomic percent additions of Fe, Al, Si, and Cr to Ni_4Mo in which a Ni to Mo ratio of four to one was maintained was studied. X-ray diffraction measurements were used to determine the long range order parameter in these alloys. Hardness measurements and metallographic studies were also made.

The four additions decreased the ordering rate slightly. An increase in the amount of the addition (from 0.5 to 1.0 %) caused a decrease in the ordering rate. The ordering rate increased for all alloys as the aging temperature was increased.

TABLE OF CONTENTS

SECTION	PAGE
1. INTRODUCTION	1
2. LITERATURE SURVEY	3
3. THEORETICAL BACKGROUND	15
4. EXPERIMENTAL PROCEDURE	23
5. RESULTS AND DISCUSSION	26
6. CONCLUSIONS AND RECOMMENDATIONS	50
REFERENCES	52
APPENDIX	57
VITA	92

LIST OF TABLES

TABLE		PAGE
A.1.	Integrated intensities after aging 0.5 h. at 650°C.....	76
A.2.	Integrated intensities after aging 1 h. at 650°C.....	77
A.3.	Integrated intensities after aging 2 h. at 650°C.....	78
A.4.	Integrated intensities after aging 4 h. at 650°C.....	79
A.5.	Integrated intensities after aging 8 h. at 650°C.....	80
A.6.	Integrated intensities after aging 24 h. at 650°C.....	81
A.7.	Integrated intensities after aging 0.1 h. at 700°C.....	82
A.8.	Integrated intensities after aging 0.25 h. at 700°C.....	83
A.9.	Integrated intensities after aging 0.5 h. at 700°C.....	84
A.10.	Integrated intensities after aging 1 h. at 700°C.....	85
A.11.	Integrated intensities after aging 2 h. at 700°C.....	86
A.12.	Integrated intensities after aging 4 h. at 700°C.....	87
A.13.	Integrated intensities after aging 8 h. at 700°C.....	88
A.14.	Integrated intensities after aging 24 h. at 700°C.....	89
A.15.	Integrated intensities after aging 48 h. at 700°C.....	90
A.16.	Integrated intensities after aging 15 h. at 775°C.....	91

LIST OF FIGURES

FIGURE		PAGE
2.1.	Ni-Mo Phase Diagram	7
2.2.	Diagram for the Ni-Mo-Fe system at 860°C	12
5.1.	Long range order parameter of samples with Cr addition	29
5.2.	Long range order parameter of samples with Si addition	30
5.3.	Long range order parameter of samples with Fe addition	31
5.4.	Long range order parameter of samples with Al addition	32
5.5.	Long range order parameter of pure Ni_4Mo sample.	33
5.6.	Long range order parameter of samples with 1 at.% alloy addition, aging temperature 700°C	34
5.7.	Long range order parameter of samples with 1 at.% alloy addition, aging temperature 650°C	35
5.8.	Long range order parameter of samples with 0.5 at.% alloy addition, aging temperature 700°C	36
5.9.	Long range order parameter of samples with 0.5 at.% alloy addition, aging temperature 650°C	37
5.10.	The 0.5 at.% Si sample as quenched, 200X	43
5.11.	The 0.5 at.% Si sample as quenched, 500X	43
5.12.	The 1 at.% Si sample after aging 4 h. at 700°C, 500X	44
5.13.	The 0.5 at.% Si sample after aging 4 h. at 700°C, 500X	44
5.14.	The 1 at.% Si sample after aging 8 h. at 700°C, 500X	45
5.15.	The 0.5 at.% Si sample after aging 8 h. at 700°C, 500X	45

FIGURE PAGE

5.16. The 1 at.% Si sample after aging 48 h. at 700°C, 500X..... 46

5.17. The 0.5 at.% Si sample after aging 48 h. at 700°C, 500X..... 46

A.1. Hardness of samples with Cr addition, aging temperature 750°C..... 58

A.2. Hardness of samples with Cr addition, aging temperature 700°C..... 59

A.3. Hardness of samples with Cr addition, aging temperature 650°C..... 60

A.4. Hardness of samples with Si addition, aging temperature 750°C..... 61

A.5. Hardness of samples with Si addition, aging temperature 700°C..... 62

A.6. Hardness of samples with Si addition, aging temperature 650°C..... 63

A.7. Hardness of samples with Fe addition, aging temperature 750°C..... 64

A.8. Hardness of samples with Fe addition, aging temperature 700°C..... 65

A.9. Hardness of samples with Fe addition, aging temperature 650°C..... 66

A.10. Hardness of samples with Al addition, aging temperature 750°C..... 67

A.11. Hardness of samples with Al addition, aging temperature 700°C..... 68

A.12. Hardness of samples with Al addition, aging temperature 650°C..... 69

A.13. Hardness of samples with 1 at.% alloy addition, aging temperature 750°C..... 70

A.14. Hardness of samples with 1 at.% alloy addition, aging temperature 700°C..... 71

FIGURE PAGE

A.15. Hardness of samples with 1 at.% alloy addition, aging temperature 650°C..... 72

A.16. Hardness of samples with 0.5 at.% alloy addition, aging temperature 750°C..... 73

A.17. Hardness of samples with 0.5 at.% alloy addition, aging temperature 700°C..... 74

A.18. Hardness of samples with 0.5 at.% alloy addition, aging temperature 650°C..... 75

1. INTRODUCTION

In several binary systems, there occurs an order-disorder reaction at compositions at or near to a stoichiometric composition. Below some temperature, called the critical temperature, T_c, each site in the unit cell is correctly occupied by a particular atomic species. This state in which the ordered unit cell is repeated over long distances is known as long range order (LRO). If all sites are filled with the correct atomic species, the LRO is perfect.

Upon heating above T_c, the long range order breaks down. Some systems exhibit a state of short range order (SRO) above T_c. In this state, atoms are not randomly distributed on the lattice, but tend to have non-statistically large numbers of unlike atoms as nearest neighbors. There is, however, no long period order. Other systems take a random state above T_c. In this case, the probability that a lattice site is occupied by a particular species is equal to the concentration of that species in the phase.

Order-disorder transitions are in general accompanied by anomalous behavior of properties such as the electrical resistivity and the specific heat. The transition can also be detected by x-ray diffraction, since ordering gives rise to extra reflections in the diffraction pattern.

A series of commercially important alloys, the Hastelloy B series, is based on the Ni_4Mo composition in the Ni-Mo system. An ordering reaction occurs at this composition at the temperature of 868°±5°C. Above T_c, the α-phase, a FCC solid solution, exists. Below

the critical temperature, long range ordering occurs; this results in the formation of the β-phase, which has a BCT unit cell. The sublattices are BCT: one is occupied by Mo atoms and four are occupied by Ni atoms. As the β-phase is brittle, its presence in the Ni_4Mo base commercial alloys is undesirable.

The formation of the β-phase in Hastelloy B has been suppressed by the addition of 5% Fe. In Hastelloy B-2, the $\alpha \rightarrow \beta$ reaction has been slowed by a 2% Fe addition; the reaction has not, however, been suppressed. In this investigation, the effect of smaller Fe additions and of other third elements on the formation of the β-phase have been studied. Fe, Cr, Si, and Al have been added in the amounts of 0.5 and 1.0 atomic percent (at.%) to a Ni-Mo base. The Ni to Mo ratio has been maintained at four to one (4:1).

X-ray diffraction and hardness measurements have been used to determine the effect of these additions on the extent and kinetics of the ordering reaction.

2. LITERATURE SURVEY

2.1 Introduction

The existence of long range order in metals was first hypothesized by Tammann [53] following studies concerning the resistance of Cu-Au alloys to attack by nitric acid. When the Au/Cu ratio was greater than or equal to one, the alloy was not attacked. Tammann attributed this behavior to the existence of atomic planes containing only Au atoms alternating with planes of Cu atoms (hence an ordered structure).

In a series of studies of the Cu-Au and Cu-Zn alloy systems, Bain [2,3,4] confirmed the existence of long range order at some compositions of these alloys by x-ray diffraction. He concluded that extra lines in the x-ray diffraction patterns implied that, in addition to the space lattice of the binary alloy, each atomic species had its own space lattice and that the atoms were hence arranged in a specific order.

Bragg and Williams [8] presented the first theoretical treatment of long range order, which was based on statistical mechanics. They introduced the long range order parameter, S. Additional theoretical work by Bethe [6] led to the short range order parameter, α.

A review of the theory to 1937 and a discussion of the effect of order on various properties was given by Nix [43]. Since, several books and proceedings of conferences concerning the theoretical aspects of order-disorder phenomena have been published. Green [23] considered order-disorder phenomena using statistical mechanics and a two

dimensional Ising model. The theory of order-disorder phenomena in alloys has been discussed by Krivoglaz and Smirnov [35] and in the proceedings of a symposium on the subject [56].

Reviews concerning the effect of the order-disorder transition on material properties such as mechanical, electrical, magnetic, and chemical have been presented by Stoloff and Davies [52] and Cohen [16].

In addition, the results of numerous studies of particular order-disorder systems have been published. Those concerning the Ni-Mo system or those presenting aspects of interest to the present study will be discussed below.

2.2 The Ni-Mo Phase Diagram

The first phase diagram of the Ni-Mo system was published by Grube and Schlect [24]. The diagram was based on their resistivity, hardness, x-ray, and microstructural investigations, on previous thermal and microstructural investigations made by Baar and confirmed by Dreibholz, and on hardness measurements made by Koster and Schmidt (all first reported in [24]). Grube and Schlect were unable to define the region below ~880°C and between ~30-60 wt.% Mo fully. This region was later completed by Grube and Winkler [25].

The second complete Ni-Mo phase diagram, based on metallographic and x-ray data, was published in 1942 by Ellinger [20]. Some corrections to the high temperature region of this diagram were proposed by Bloom in 1954 [7]. A phase diagram compiled from these and other data available in the literature was published in the Constitution of Binary Alloys [27].

Guthrie and Stansbury [26] produced a partial phase diagram (18-62 wt.% Mo and 600-1000°C) constructed from microstructural, x-ray, and hardness data. The β peritectoid temperature was established at 868°±5°C and the γ peritectoid temperature at 910°±5°C. The α phase boundary was also changed with respect to that proposed by Ellinger. The diagram in the Constitution of Binary Alloys, First Supplement, [21] was amended to include this and other work done for the AEC and the work of two Russian researchers.

A fifth complete phase diagram was published by Casselton and Hume-Rothery [9]. Their work was based on their thermal, microstructural, and x-ray measurements and on the diagram published by Hansen. These authors maintain that the β-phase extends from 80.5 to 81.0 at.% Ni and does not include the exact stoichiometric composition Ni_4Mo.

Kozlov and Kushavenko [34] reheated completely ordered samples of composition 20.7 at.% Mo in order to determine the critical temperature, which they placed at 876°±3°C. They found their samples to be on the low-Mo side of the peritectoid congruence point, indicating that the congruence point is not at the stoichiometric composition. (This work places the congruence point on the Mo-rich side as opposed to Casselton's work [9] which places it on the Ni-rich side.)

In summary, the Ni-Mo system at low temperature (<~870°C) is comprised of the Ni-rich terminal solid solution α, the stoichiometric phases β (Ni_4Mo), γ (Ni_3Mo), δ (NiMo), and the Mo-rich terminal solid solution ϵ. The Ni-Mo phase diagram, compiled from those in Constitution of Binary Alloys [27] and Constitution of Binary Alloys, First

Supplement, [21] is shown in Figure 2.1. A metastable phase Ni_2Mo has been observed on quenching from the α to the $\beta + \gamma$ regions [50].

2.3 The Structure of Ni_4Mo

Grube and Schlect [24] first reported the existence of the β-phase and classified it as FCT with a c/a ratio of 0.986. Harker [28] presented an extensive study of Ni_4Mo in 1944. He concluded that the $\alpha + \gamma \rightarrow \beta$ peritectoid reaction was an FCC → BCT structure change and classed Ni_4Mo in the space group I4/m. He determined the lattice parameters as a_0 = 5.720 Å and c_0 = 3.564 Å, c/a = 0.6231. He also defined the orientations that the BCT unit cell can take with respect to the FCC high temperature phase as follows:

1. The BCT c-axis can take any of three cube directions;
2. The BCT a-axis is at a small positive or negative angle to the cube directions;
3. The BCT cell can have its origin at five positions.

This yields a total of 3 x 2 x 5 = 30 ways in which the BCT cell can form from the FCC matrix, but there are, however, only six unique orientations. The lattice parameters were redetermined by Guthrie and Stansbury [26] to be a_0 = 5.727 Å and c_0 = 3.566 Å, c/a = 0.623, confirming Harker's results. Casselton and Hume-Rothery [9] determined the lattice parameters of the BCT cell as a_0 = 5.683 Å and c_0 = 3.592 Å, c/a = 0.632.

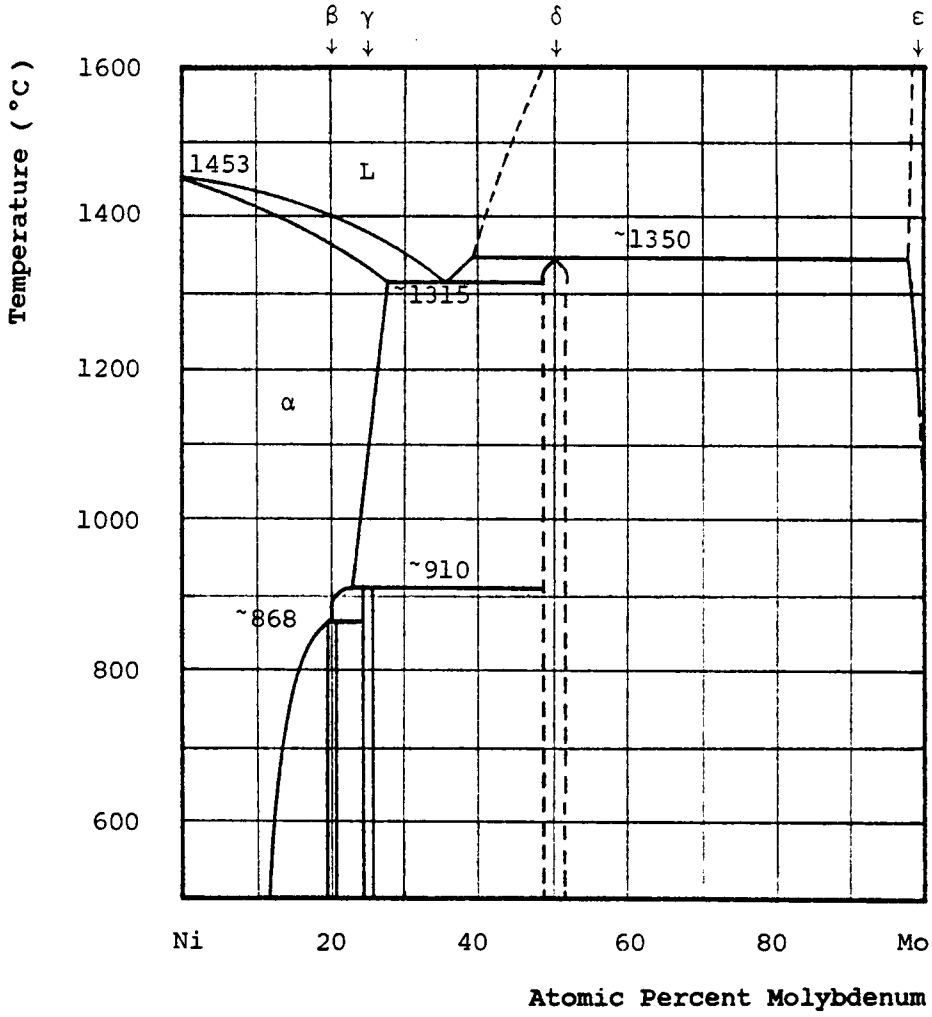


Figure 2.1. Ni-Mo Phase Diagram.

2.4 Short Range Order in the α-Phase

The nature of the short range ordered state which occurs in the α-phase at the Ni_4Mo composition has been the subject of many papers in recent years. Spruiell and Stansbury [51] studied the diffuse intensity in the $h_1, h_2, 0$ plane of reciprocal space for Ni-20 at.% Mo and Ni-10.7 at.% Mo single crystals using x-ray diffraction techniques. Intensity maxima indicating the presence of short range order (SRO) were found at the {1,1/2,0} positions in samples quenched from 1000°C. Reheating the Ni-20 at.% Mo samples for one hour at 650°C caused the maxima to split into peaks. These peaks occurred near superlattice reflections. These authors concluded that this indicated the existence of a domain structure in the alloy. The minimum domain size for which splitting could be seen was calculated to be $10a_0$ ($\sim$36Å).

Clapp and Moss [15, 41] have advanced an explanation of the {1,1/2,0} diffuse scattering maxima using a statistical theory model. They successfully predicted the positions of these maxima using their model. Because the disordered and partially ordered alloys have different diffraction patterns, the microdomain model is discounted by these authors.

These two papers have engendered two schools of thought concerning the nature of SRO in Ni_4Mo. The first paper provides the basis for the "microdomain theory" in which the assumption is made that small ordered domains exist in the disordered matrix above T_c and provide nuclei for the long range ordered structure below T_c. The second paper

gives rise to the "statistical theory" in which it is assumed that statistical considerations only explain the presence of SRO.

Many researchers have attempted to prove or disprove one of these two theories explaining the {1,1/2,0} diffuse maxima. The articles concerning the nature of the α-phase are numerous [42, 48, 36, 49, 45, 18, 33, 11, 12, 13, 19, 55, 54]. At present, the controversy remains unresolved.

2.5 The Order-Disorder Transition

The mechanism and kinetics of the short range to long range order transition have also been studied by many authors. Ruedl et al. [48] presented the first extensive electron microscope investigation of Ni_4Mo in which the effect of planar defects--anti-phase boundaries, anti-parallel twins, and perpendicular twins--on the diffraction pattern was discussed.

Chakravarti et al. [10] have studied ordering mechanisms in poly-crystalline Ni_4Mo during annealing at 700°C. X-ray diffraction, electron microscopy, field ion microscopy, and mechanical property tests were used. Their results support a homogeneous ordering mechanism in which "the frequency of nucleation is so high and the nuclei so small that impingement between the domains is instantaneous" [10, p. 402]. They observed gradual broadening and splitting of the fundamental reflections which was interpreted to indicate a homogeneous ordering mechanism. The process was divided into two stages. The first, when the long range order parameter, S, was smaller than 0.7, was attributed to ordering within the domains. The second, for which S was greater than

0.8, was characterized by the reduction of domain boundaries. Empirical equations describing the two stages were given. In a later paper [40], these authors used the same technique to study the transformation at 650°C. They found the kinetics of ordering and domain growth to be significantly slower at this lower temperature.

Artsishevskaya et al. [1] studied the ordering process of Ni-Mo alloys by electron microscopy and x-ray diffraction. They studied the reaction at temperatures of 600, 700, and 800°C and for times of ten minutes to one hundred hours. They characterized the ordering process as "slow" since ordered and disordered phases were seen to coexist to at least one hundred hours at annealing temperatures of 700 and 800°C. They found that the annealing temperature affected the size and shape of domains and perpendicular twins.

Kiriyenko and Potapov [32] used field ion microscopy to study ordering mechanisms in Ni-Mo alloys. The mechanism was found to be primarily heterogeneous at high temperatures (800°C for ~18 at.% Mo) and homogeneous at lower temperatures (700°C). They hypothesized that the degree of undercooling affected the mechanism. They also noted that as the composition departed from stoichiometric, the homogeneous mechanism became more important. This was attributed to the lower critical temperature at non-stoichiometric compositions.

2.6 Order Hardening

An important phenomenon which occurs in order-disorder alloys which undergo a structural change upon ordering is order hardening.

Harker [29] first discussed this effect, basing his observations on a study of the AuCu alloy.

Chakravarti et al. [10] studied order hardening in Ni_4Mo. They attributed the strength increase to the domain size and the tetragonal distortion which occurs when the Ni_4Mo composition orders. They related the concurrent decrease in ductility to either "the development of dislocations in co-planar arrays or concentrated slip in the heterogeneous component" [10, p. 403].

Ling and Starke [39] found that the hardness and rms strain measured during the ordering process correlated with the LRO parameter. This is due to the constant decrease in the size of the c-axis. However, this was found not to be the only source of hardening since the hardness did not begin to decrease when the alloy was fully ordered. (If lattice strain at the boundaries is the only source of strain, domain growth would cause a fall in the hardness.) They attributed the continued increase in hardness to dislocations generated at points of lattice strains at interfaces.

2.7 Ternary Systems

Of the ternary systems (Ni-Mo + Fe, Cr, Al, or Si) studied in this research the Ni-Mo-Fe system is the sole system to have been investigated to any extent.

Norem [44] studied this system and prepared isothermal sections of the Ni-rich corner for temperatures of 700, 800, 860, and 900°C. The section for 860°C, adapted from Norem, is shown in Figure 2.2. In

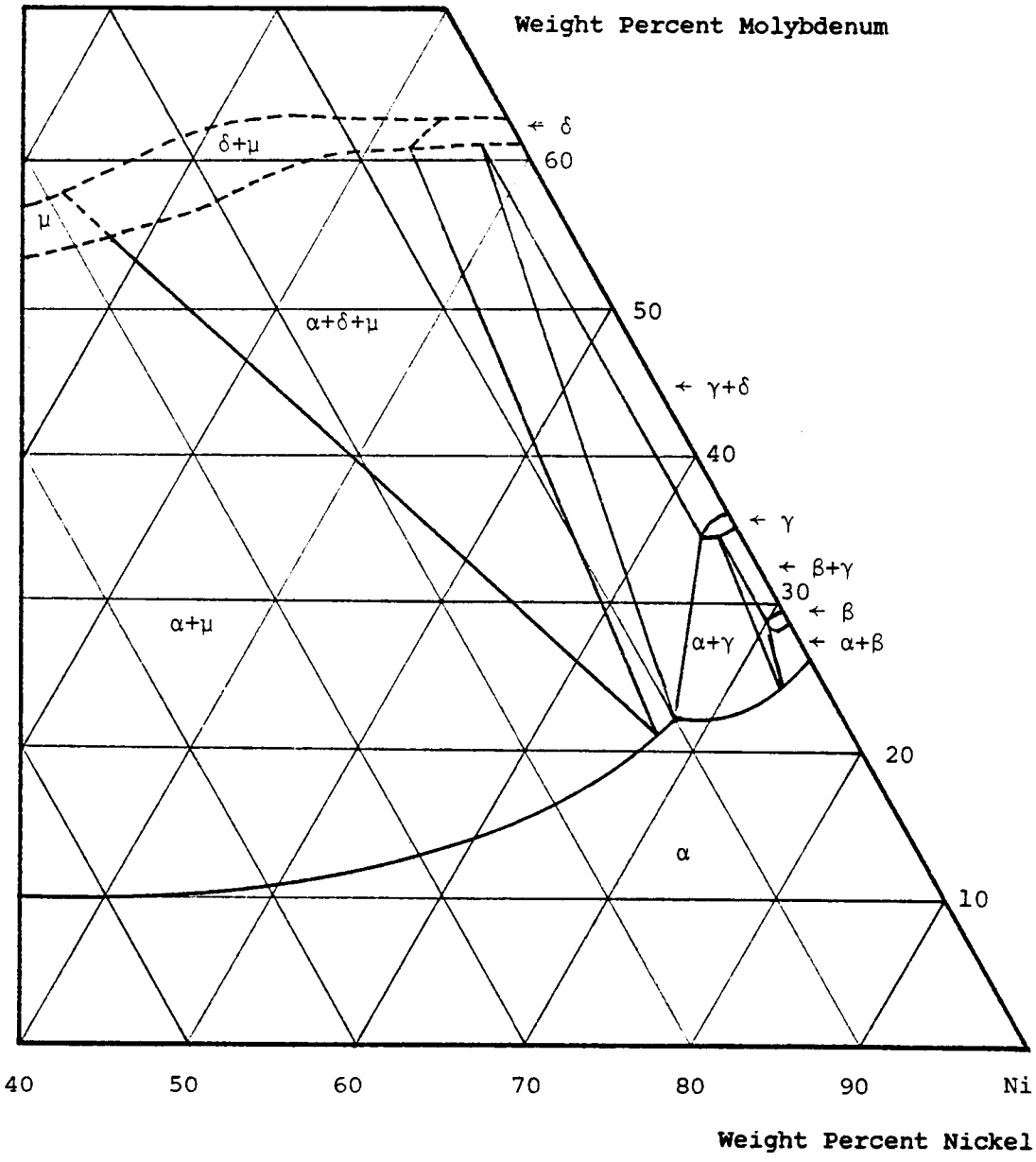


Figure 2.2. Diagram for the Ni-Mo-Fe system at 860°C.

addition, an isothermal section of the system at 1200°C has been prepared by Das et al. [17].

Lei [38] investigated the effect of 0-8 wt.% Fe additions to the Ni-Mo system (Ni:Mo = 4:1) using electrical resistivity measurements, hardness measurements, and transmission electron and optical microscopy. He found the solubility of Fe in the β-phase to decrease with increasing temperature and determined the following points: 4.5 wt.% at 600°C, 3.2 wt.% at 700°C, 1.3 wt.% at 800°C, 0.3 wt.% at 850°C, and 0 at 868°C. He also found that the addition of Fe slows the ordering transformation.

High temperature isothermal sections (1200 and 1250°C) of the Ni-Mo-Cr ternary systems are available [47, 7], but no low temperature sections have been prepared. No information concerning the Ni-Mo-Al or Ni-Mo-Si systems was found.

The effect of additions of Nb and V to Ni_4Mo has been the subject of investigations by several Russian researchers. Kiriyenko et al. [31] hypothesized that the improved corrosion resistance of Ni_4Mo + Nb or V was due to the effect of these elements on the ordering process. Using x-ray diffraction, hardness measurements, and field ion microscopy, they studied the effect of 2.09-2.39 at.% V and of 1.34 at.% Nb additions to Ni_4Mo. V was found to slow the ordering process, the effect being more important at elevated temperatures (>800°C). This high temperature behavior was attributed to the effect of V on the ternary phase diagram, specifically, to the broadening of the α + Ni_3Mo range and the depression of the critical temperature for Ni_4Mo formation. Although the appearance of Ni_4Mo was retarded, the mechanical

properties of the alloy with added V were nonetheless degraded due to the appearance of Ni_3Mo, which is brittle. The effect of Nb addition was similar, but the results were less clear.

Potapov et al. [46] added 5.5 and 9.9 at.% W to Ni-13 at.% Mo alloys and studied these alloys by electron diffraction, field ion microscopy, and x-ray diffraction. The alloys were annealed at 800 and 700°C and the phases present after various times were discussed. When the 9.9% W alloy was quenched from above T_c, the observed phases were the α solid solution, a BCC W-based phase, and regions of short range ordered $Ni_4(Mo,W)$ and $Ni_2(Mo,W)$. The {1,1/2,0} electron diffraction diffuse intensities were visible in the quenched structure and sharpened after annealing at 800°C for five minutes. These reflections disappeared after thirty minutes. After four to ten hours at 800°C, the $Ni_2(Mo,W)$ phase disappeared completely. The alloy of lower W content behaved similarly, but did not exhibit the BCC W-based phase. The transformation at 700°C was comparable although slower.

3. THEORETICAL BACKGROUND

3.1 Order-Disorder and X-Ray Diffraction Theory

Any given plane of atoms is statistically the same as any other plane in a disordered solid solution. However, in an ordered solid solution, a given plane can differ in composition from a plane parallel to it. For example, the composition of alternate planes of a given family could be such that one consists of A atoms and the other of B atoms. This reduces the average symmetry of the solution and hence gives rise to extra reflections in the diffraction pattern. These lines are known as "superlattice lines" [5].

The degree of long range order of a material is expressed by the parameter S, which is equal to one when order is complete (and the composition of the material is stoichiometric) and is equal to zero when there is no order—that is, for a random solid solution. An expression for S will now be developed.

Consider a composition in a binary system of elements A present in fraction x_A and B present in fraction x_B (where $x_A + x_B = 1$). Call α sites the atomic positions occupied by A atoms and β sites the atomic positions occupied by B atoms when there exists perfect long range order in a stoichiometric AB compound. The fractions of the α and β sites are called y_α and y_β, respectively. Then define the parameters r_α as the fraction of α sites occupied by the right atom (i.e., an A atom) and w_α as the fraction of α sites occupied by the wrong atom (i.e., a B atom). The parameters r_β and w_β are defined similarly. Four important relations follow from these definitions:

$$r_\alpha + w_\alpha = 1$$

$$r_\beta + w_\beta = 1$$

$$y_\alpha r_\alpha + y_\beta w_\beta = x_A$$

$$y_\beta r_\beta + y_\alpha w_\alpha = x_B.$$

Expressions for the long range order parameter S can now be defined:

$$S = r_\alpha + r_\beta - 1 = r_\alpha - w_\beta = r_\beta - w_\alpha$$

or

$$S = \frac{r_\alpha - x_A}{y_\beta} = \frac{r_\beta - x_B}{y_\alpha}.$$

These expressions also apply when the composition of the binary solution is nonstoichiometric.

The structure factor F consists of a summation over the α sites of the unit cell and a summation over the β sites of the unit cell:

$$F = \sum_\alpha (r_\alpha f_A + w_\alpha f_B) e^{2\pi i(hx_n + ky_n + \ell z_n)} + \sum_\beta (r_\beta f_B + w_\beta f_A) e^{2\pi i(hx_n + ky_n + \ell z_n)}. \qquad (3\text{-}1)$$

Using the relations given above, the structure factor can be expressed in terms of atom fractions (x_A and x_B) or in terms of S for the various combinations of hkl (i.e., even, odd, mixed, etc.). Combinations of hkl for which S appears in the structure factor are superlattice reflections.

In summary, the relation of the integrated intensities, E^F and

E^S, of the fundamental and superlattice reflections, respectively, to the degree of order, S, is as follows. The fundamental reflections are independent of the degree of order. That is, for S ranging from 0 to 1 (a random to a completely ordered solid solution),

$$E^F_{RANDOM} = E^F_{LRO}.$$

For a random solid solution, there are no superlattice reflections:

$$E^S_{RANDOM} = 0.$$

More generally, the intensity of a superlattice reflection is equal to the intensity of the superlattice reflection of a completely ordered alloy times S^2:

$$E^S = E^S_{LRO} \cdot S^2.$$

(The preceding discussion is based on Warren [57, pp. 208-209].)

3.2 The Structure Factor of Ni_4Mo

The calculation of the structure factor of Ni_4Mo is now given. Ordered Ni_4Mo has been classed in the I4/m space group with two Mo atoms in the (000) [+ BC translations] positions and eight Ni atoms in the (xy0), ($\bar{x}\bar{y}$0), ($\bar{y}$x0), and (y$\bar{x}$0) [+ BC translations] positions [28, 30]. Harker found the values for x and y to be x = 2/5 and y = 1/5. Thus, the Mo atoms are positioned at (000) and (1/2 1/2 1/2) and the Ni atoms are at (0.4 0.2 0), (-0.4 -0.2 0), (-0.2 0.4 0), (0.2 -0.4 0), (0.9 0.7 0.5), (0.1 0.3 0.5), (0.3 0.9 0.5), and (0.7 0.1 0.5).

Using Eq. (3-1), the structure factor is, for h + k + l even,

$$F = 2\{f_{Mo} + f_{Ni}2\cos 2\pi(0.4h + 0.2k) + 2\cos 2\pi(-0.2h + 0.4k)]\} \quad (3\text{-}2)$$

and is, for h + k + l odd,

$$F = 0.$$

When values of (hkl), the sums of which are even, are substituted into Eq. (3-2), the structure factor for one group of reflections is found to be:

$$F = 2f_{Mo} + 8f_{Ni}$$

and that for the other group is:

$$F = 2S(f_{Mo} - f_{Ni}).$$

The reflections for which the structure factor is independent of S are the fundamental reflections, while those dependent upon S are the superlattice reflections. These two groups can be separated by considering the transformation from the FCC to the BCT cell. The reflections from the original FCC planes are the fundamental reflections of the BCT lattice, while the remaining reflections are the superlattice reflections.

3.3 Calculation of the Long Range Order Parameter

Factors which introduce errors into intensity calculations are extinction, microabsorption, large grain size, preferred orientation, statistical fluctuations (random error from experimental apparatus), background noise, and superposition [22]. These sources of error can in

most cases be minimized by careful experimental procedure. Then, the long range order parameter S can be found from a comparison of the fundamental and superlattice intensities at some stage of ordering, E^F and E^S, to the fundamental and superlattice intensities of a completely ordered specimen, E_o^F and E_o^S:

$$S^2 = \frac{E^S/E_o^S}{E^F/E_o^F}. \qquad (3\text{-}3)$$

Alternately, S can be found by comparing the experimental intensities to the calculated intensities:

$$S^2 = \frac{E^S/R^S}{E^F/R^F}.$$

The calculated intensity R is found using the equation:

$$R = |F|^2 p(LP)e^{-2M},$$

where p is the multiplicity factor, F the structure factor, LP the Lorentz polarization factor, and e^{-2M} the temperature factor.

In the case of superposition of fundamental and superlattice reflections, the value of S can be calculated iteratively. The procedure starts with an initial value of S computed from Eqn. (3-3), in which the effects of superposition are accounted for by considering the relative (calculated) intensities of the superimposed reflections. The value of S is then refined by successive iterations; each iteration computes a new value of S by comparing the experimental intensities to those calculated by using the previous value of S, in which the effect of superposition is accounted for. The procedure is continued until

convergence, that is, until the correction made in a step becomes less than a predetermined threshold. For extensive superposition, LeFevre and Starke [37] have developed a more complex iterative procedure and applied it to an investigation of ordering of the intermetallic compound Au_4V.

3.4 Effects of the Third Element Addition

The addition of a third element to a binary order-disorder alloy can increase, decrease, or have no effect on the rate of the ordering reaction. The influence of the addition depends upon many factors, among which are its effect on the lattice parameter and on the anti-phase domains and the lattice site which it occupies. Although there is no long range diffusion during an ordering reaction, the diffusion rate of the addition and the effect of the addition on the bulk diffusion rate plays a role in controlling the rate of the reaction.

If the reaction involves a change in lattice parameter (so that there is a bulk volume change), an addition which aids the change will increase the reaction rate and one which hinders the change will decrease the reaction rate [14]. There is a slight decrease in bulk volume from the disordered to the ordered phase of Ni_4Mo [28]. Hence, an addition which increased the lattice parameter of disordered Ni_4Mo would decrease the ordering rate. Of the additions made in this study, Al meets this criterion.

The effect of an addition on the formation and energy of the metastable network of anti-phase domain boundaries can affect the ordering rate. An addition could cause an increase in the formation of

anti-phase domains by reducing the energy at the boundary due to unlike neighbors or could stabilize the boundaries by moving into the boundaries and likewise reducing the energy. Both of these processes would reduce the ordering rate.

Although it is difficult to speculate on the effect a given addition will have on the anti-phase domain boundaries and diffusion rates, one can make a reasonable guess as to which lattice sites an addition will occupy by considering the atomic radius, the coordination number, and the electron shell configuration of the addition.

Fe is very close in size to Ni, has two free conduction electrons, as does Ni, and, at least in a small temperature range, has the same coordination number. The Fe-Ni phase diagram shows an enlarged austenite region in which there is continuous solid solubility and a low temperature ordered phase, Ni_3Fe. The Fe-Mo phase diagram shows several intermetallic compounds. One may conclude that it is likely that Fe substitutes for Ni in Ni_4Mo.

Cr is close in size to Ni and smaller than Mo. Cr and Mo are in the same periodic family and are both BCC. The Cr-Mo phase diagram shows continuous solid solubility with a solid miscibility gap. The Cr-Ni diagram indicates more complex behavior, including the formation of a low temperature ordered phase, Ni_3Cr. It is more probable that Cr substitutes for Mo in Ni_4Mo.

The Al-Mo and Al-Ni phase diagrams are both complex: Al forms several intermetallic compounds with both Ni and Mo. Atomic radius is probably the determining factor in the case of Al since it is larger

than both Ni and Mo. Al probably substitutes for Mo to minimize the size effect.

Likewise, Si forms many intermetallics with Ni and Mo and is smaller than both. Si probably substitutes for Ni to minimize the size effect.

If other considerations are equal, an addition which substitutes for Mo would be more effective in retarding ordering since there are fewer Mo lattice sites. An addition with no preferential lattice site would be least effective. So, according to this criterion and the conclusions reached above, Cr and Al, in the Mo sites, would be more effective in reducing the ordering rate than Fe and Si, in the Ni sites.

Another point which must be considered is the effect of the addition on the critical temperature and the concomitant effect on the position of the transformation curve. It is possible that the third element addition would lower the entire transformation curve so that, for measurements at a given temperature below the "nose" of the diagram, the transformation would occur more quickly in samples with an addition than without. This is not the case for Fe. Lei [38] found that although small additions of Fe decreased the critical temperature and the ordering rate at a given temperature above the nose of the diagram, there was no appreciable effect on the transformation rate at temperatures below the nose. This effect may, however, occur in the other alloys.

4. EXPERIMENTAL PROCEDURE

4.1 Alloy Preparation

The eight alloys, containing 0.5 or 1.0 atomic percent Fe, Cr, Si, or Al, were made by adding high purity Fe, Cr, Si, or Al to a Ni-Mo base alloy prepared by the Stellite Division. Mo was added to the melt to obtain a Ni:Mo ratio of 4:1. Ingots of approximately 250 g. were melted in recrystallized alumina crucibles in a Balzars induction furnace under an Ar-5%H_2 atmosphere. Four of the ingots were remelted in an arc furnace in a water cooled Cu mold in order to remove excess porosity. The ingots were then homogenized in H_2 for 100 h. at 1200°C. The pure Ni_4Mo sample used in the x-ray diffraction studies was prepared by Lei [38].

4.2 Specimen Preparation

Specimens for x-ray diffraction studies were prepared by grinding approximately 4 g. of powder from the ingots using an electric hand-held grinder with alumina grinding points. The portion of the powder which passed through a 100 mesh (150 μm) sieve was pressed into 0.5" diameter pellets. The pellets were sintered under an H_2 atmosphere for eight hours at 1000°C.

Specimens for microstructural and microhardness studies were prepared by swaging or rolling the ingots to 0.25" diameter rods. Intermediate annealing treatments were given at 1000°C in Ar as required.

4.3 Heat Treatments

Specimens for x-ray diffraction were aged at 650°C for 0.5, 1, 2, 4, 8, and 24 hours and at 700°C for 5, 15, and 30 minutes and 1, 2, 4, 8, 24, and 48 hours. Microstructural and microhardness specimens were aged at 650°C for 0.5, 1, 2, 4, 8, 24, and 48 hours; at 700°C for 0.5, 1, 2, 4, 8, 24, and 48 hours; and, at 750°C for 0.5, 1, 2, 4, 8, and 24 hours. The specimens were sealed in Vycor tubes evacuated to ~20 μm Hg for heat treatment.

4.4 X-Ray Diffraction Measurements

The integrated intensities of the (211) fundamental peak and the (110), (101), and (200) superlattice peaks were measured with a Phillips Norelco diffractometer operating at a tube voltage of 35 kV and current of 20 mA. The angular range containing each peak was scanned at a rate of 1/4° or 1/2°/min. The background intensity was accounted for by measuring the intensity at each end of the angle, then subtracting the average value. Intensity values were read from a digital output.

4.5 Metallography and Microhardness

Heat treated specimens were mounted, ground, and polished using conventional metallographic supplies and methods. The specimens were etched by swabbing with an etchant of two parts 20% HCl to one part 10% H_2O_2. The etchant and the specimens were heated to ~50°C in hot water before etching. Microhardness tests were made on the mounted, polished

specimens using a Kentron Microhardness Tester. A diamond pyramid indenter was used with a test load of 1 kg. and a loading time of 12 s.

5. RESULTS AND DISCUSSION

5.1 Introduction

The discussion of the results is divided into five parts. First, the sources of error and data analysis are discussed. Then, the effects of the amount of addition, the type of addition, and the aging temperature, as determined from the x-ray diffraction and microhardness data, are considered. In the last part, the microstructure is discussed.

5.2 Error Analysis

The major sources of error in x-ray diffraction work were listed in Section 3.3. Of these, problems arising from extinction, microabsorption, insufficiently small grain size, and preferred orientation were eliminated by the use of samples made of very fine sintered powder. The superposition of two superlattice peaks with the fundamental peak was taken into account by using the reiterative procedure outlined in Section 3.3 to calculate the long range order parameter, S. Error introduced by statistical fluctuations of the apparatus was minimized by measuring the intensities of three superlattice reflections and averaging the results. A low superlattice peak intensity to background and fundamental peak intensity ratio was the major problem in this work. This was especially serious at short aging times where the intensity of the superlattice peaks was very small compared to the background. The problem remained significant for longer aging times for, even though the background became less important, the ratio of the superlattice to fundamental peak intensities was still small. In fact,

in a fully ordered sample, the ratio of the (200) to the (211) peaks was about 0.02. Long counting times were used to diminish the magnitude of the error. In addition, the difference in the LRO parameters calculated from the three superlattice peaks was taken into account and only reasonably close values were used in calculating the average parameter. The data from the (200) peaks was discarded most often. The three peaks together were used to compute about 65% of the data points and the (110) and (101) peaks together were used for about 30% of the points. However, the result of this small superlattice peak intensity is some scatter in the curves of the LRO parameter versus time.

Due to the scatter in the data, it was desirable to attempt an analysis of the data which would give some indication of its separability. First, an attempt was made to find the equations of the curves described by the data, thence to calculate the deviation of the data points. The data did not follow a simple polynomial or exponential law, so, rather than fit the data to a curve for which no physical basis existed, it was decided to test if the groups of data points were statistically separable. The null hypothesis test was applied: the tested hypothesis was that the mean separation of the two sets of data was zero. Student's two-sided t distribution was used.

Curves for which the confidence level was greater than 0.95 were considered "separable", those for which the confidence level was 0.8-0.95 were considered "probably separable", and those for which the confidence level was less than 0.8 were considered "inseparable". One must of course remember that these are probabilities and that "separable" curves simply have a very good chance of being separate and

"inseparable" curves are much less likely to be separate. One must also keep in mind that curves which cross at an intermediate time may not be deemed separable by this method (since only the mean is tested), nor are future trends, which may be evident to the observer, accounted for. The results will be discussed in terms of separability before proceeding to the discussion of the variables.

The data are plotted in terms of S versus t and are shown in Figures 5.1-5.9. The separability of the data concerning the amount of the addition (0.5 or 1 at.%) will be considered first. The curves for the alloys containing Cr at 700°C (Fig. 5.1) and Si at both temperatures (Fig. 5.2) are inseparable. Those for Cr at 650°C (Fig. 5.1) and Al at both temperatures (Fig. 5.4) are separable. The alloys which are separable from the Ni_4Mo at 700°C (Fig. 5.6 and 5.8) are the 0.5 and 1 at.% Si. The 0.5 and 1 at.% Cr, the 0.5 at.% Fe, and the 1 at.% Al are probably separable, and the 0.5 at.% Al is not separable from the Ni_4Mo. At 650°C (Fig. 5.7 and 5.9), the 0.5 at.% Cr and 0.5 at.% Al alloys are separable from the Ni_4Mo, the 1 at.% Cr and 0.5 at.% Fe are probably separable, and the other curves are not separable.

For the 1 at.% additions at 700°C (Fig. 5.6), the Al was probably separable from the Cr and Si. Cr and Si could not be separated. For the 1 at.% additions at 650°C (Fig. 5.7), the Si was separable from the Cr and Al. The Cr and Al were inseparable. For the 0.5 at.% additions at 700°C (Fig. 5.8), the Al was separable from the Cr and Si and probably separable from the Fe. The Cr and Fe were both probably separable from the Si. The Cr and Fe could not be separated. For the 0.5 at.%

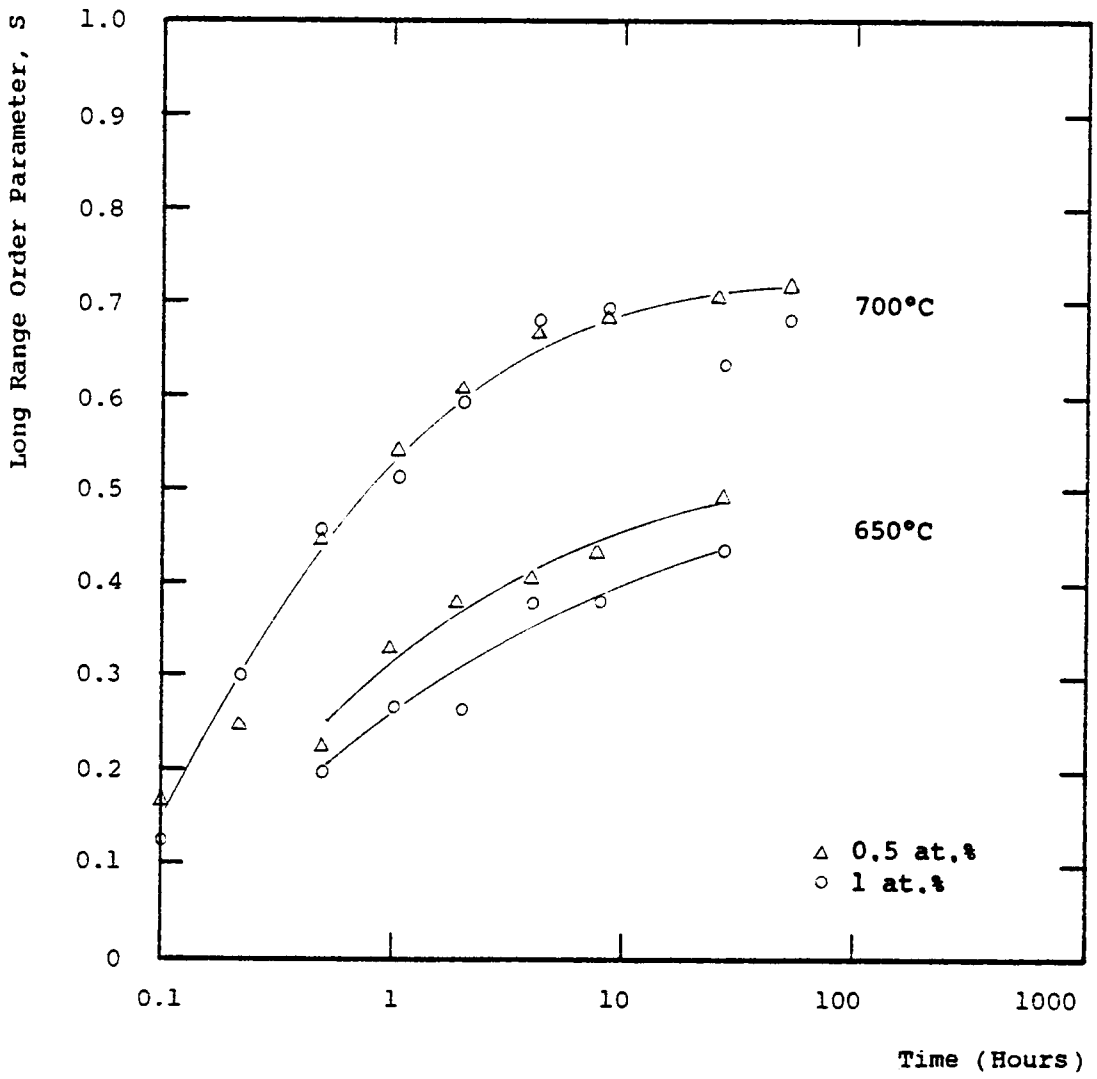


Figure 5.1. Long range order parameter of samples with Cr addition.

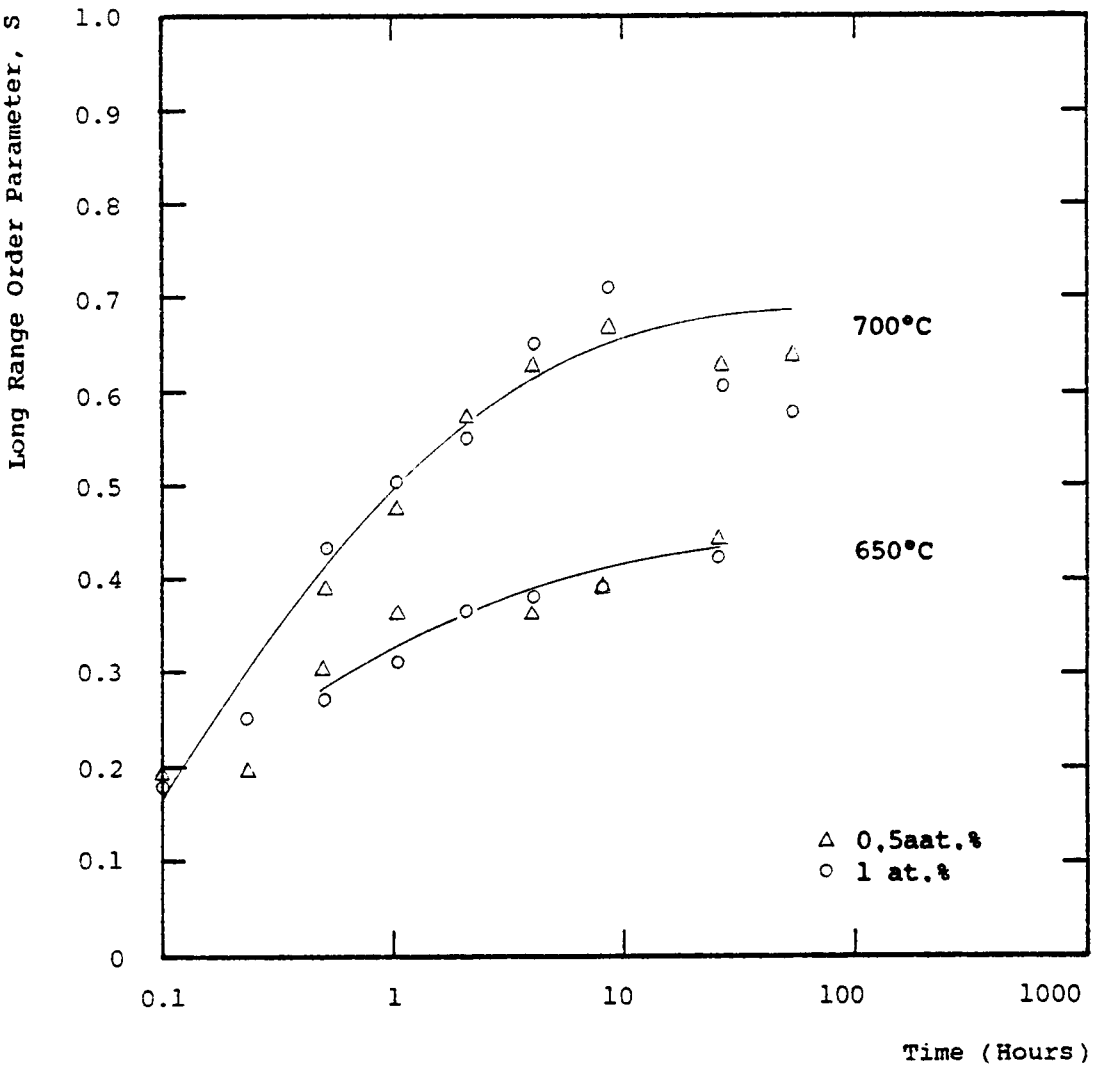


Figure 5.2. Long range order parameter of samples with Si addition.

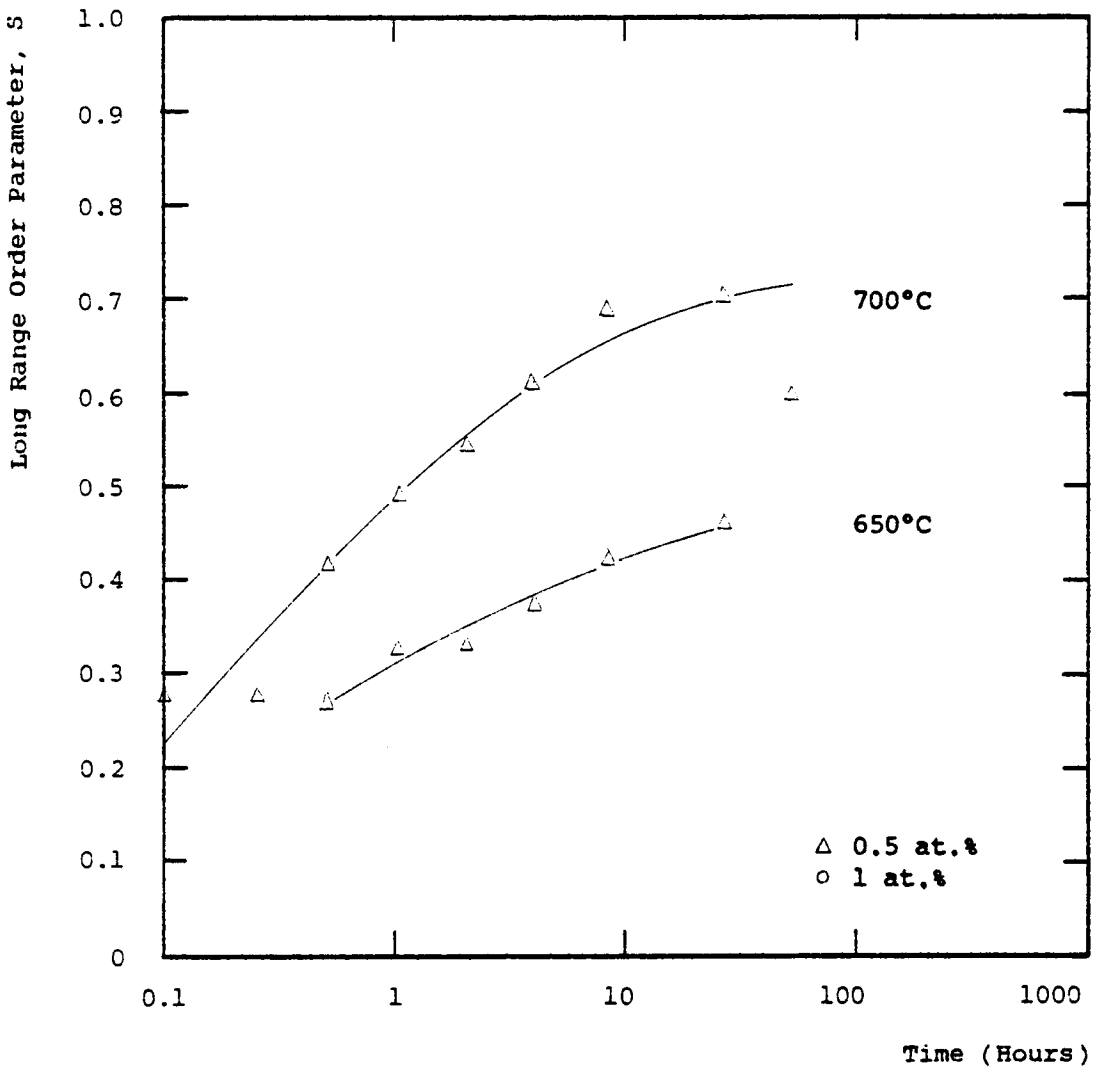


Figure 5.3. Long range order parameter of samples with Fe addition.

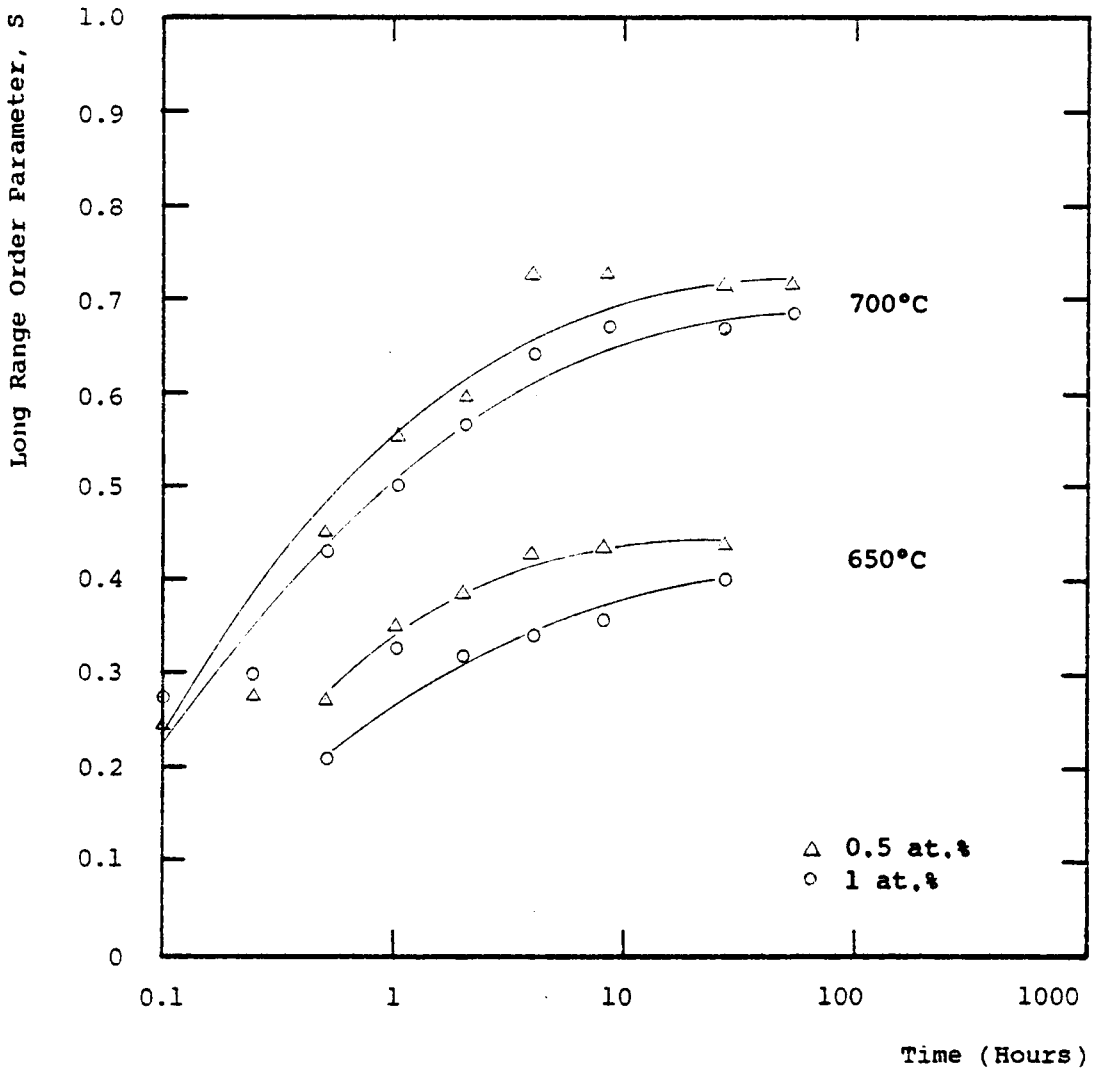


Figure 5.4. Long range order parameter of samples with Al addition.

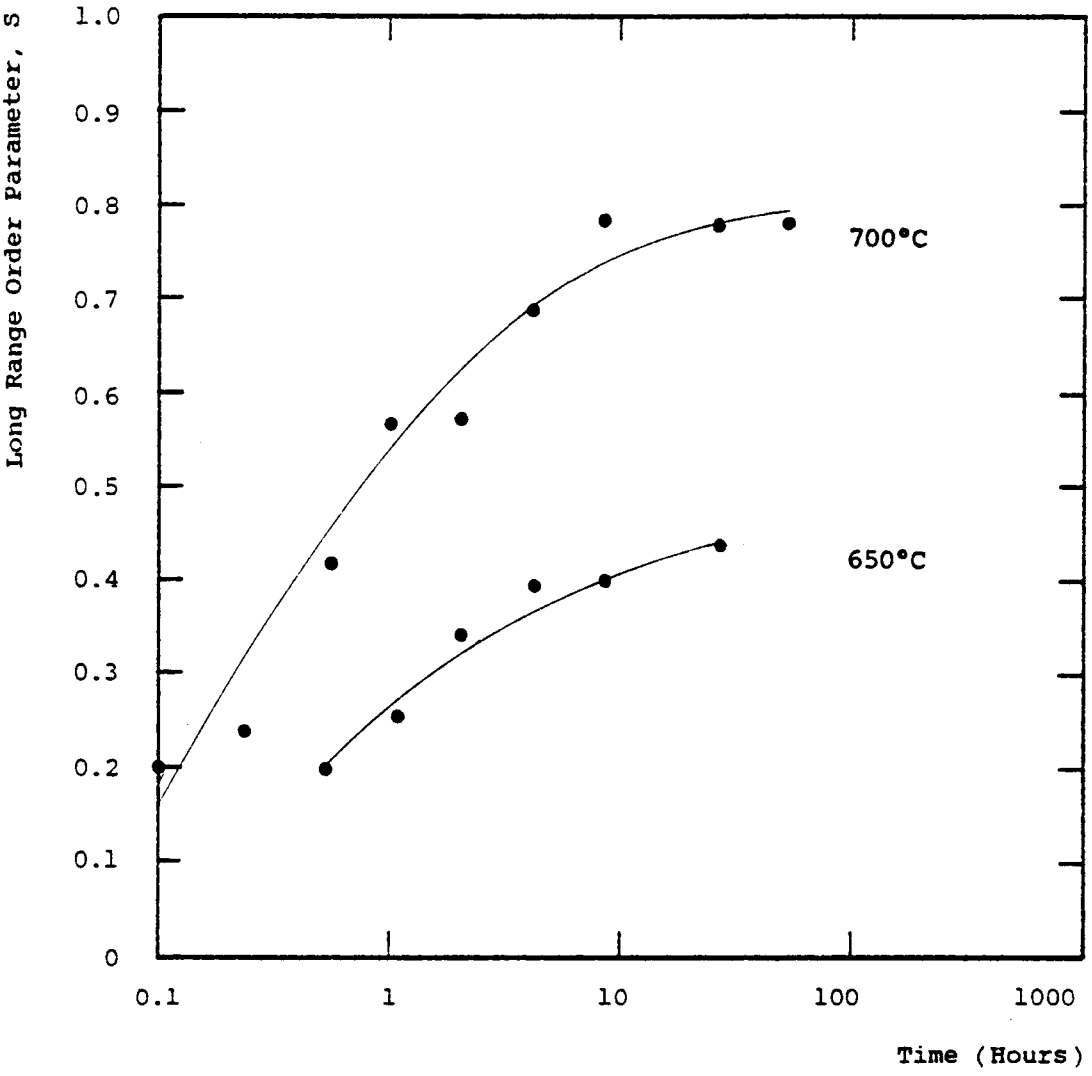


Figure 5.5. Long range order parameter of pure Ni_4Mo sample.

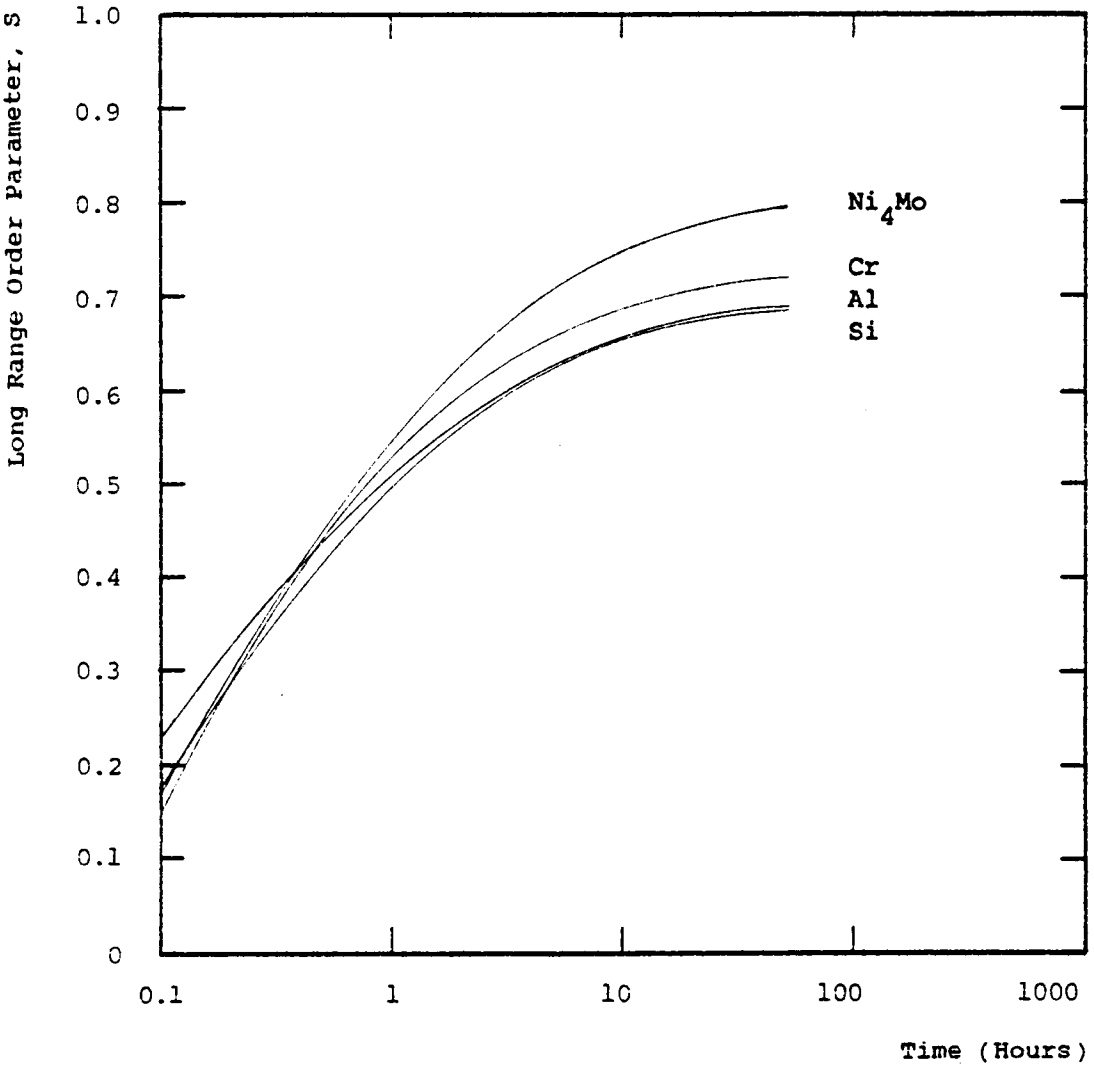


Figure 5.6. Long range order parameter of samples with 1 at.% alloy addition, aging temperature 700°C.

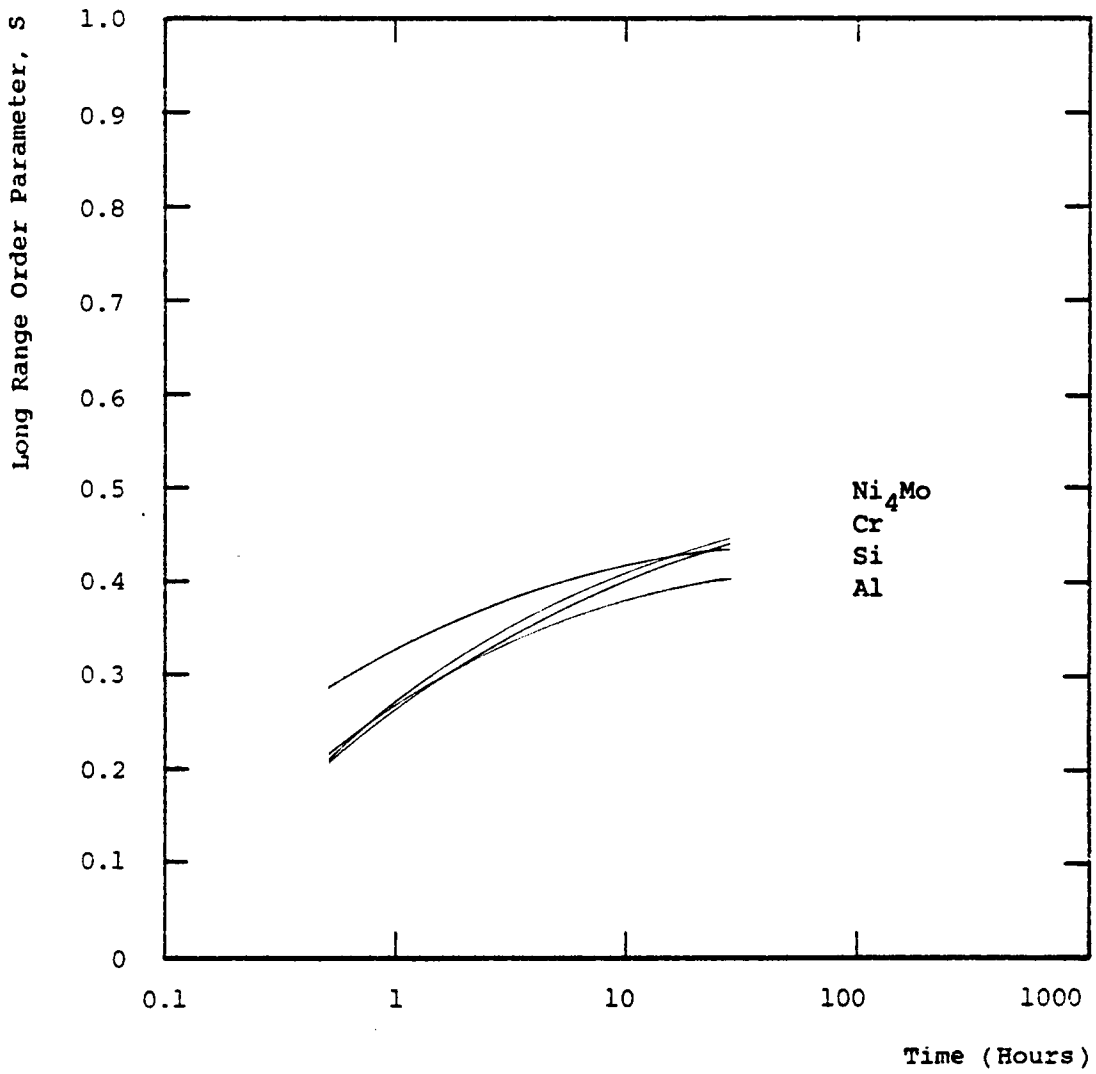


Figure 5.7. Long range order parameter of samples with 1 at.% alloy addition, aging temperature 650°C.

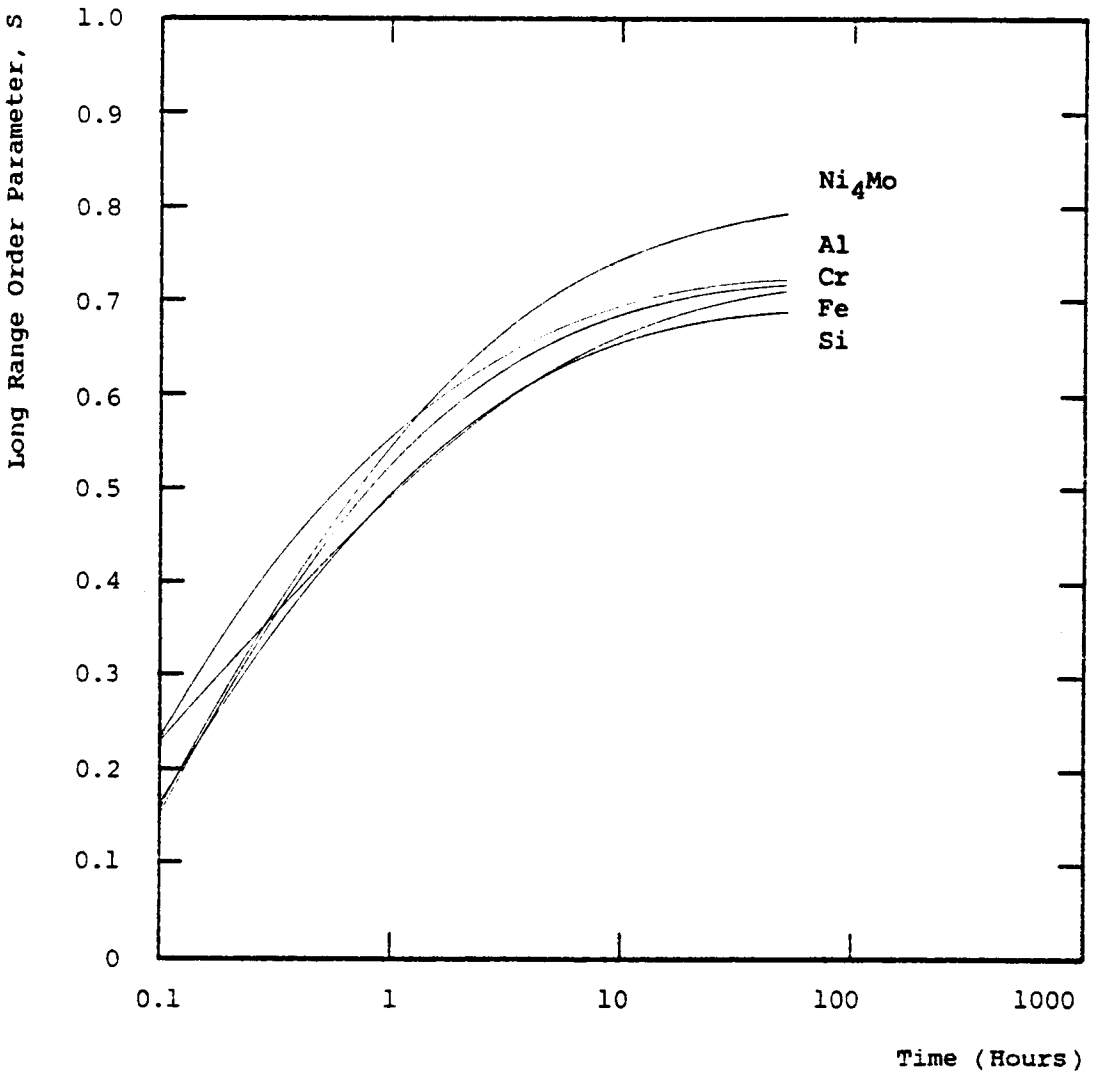


Figure 5.8. Long range order parameter of samples with 0.5 at.% alloy addition, aging temperature 700°C.

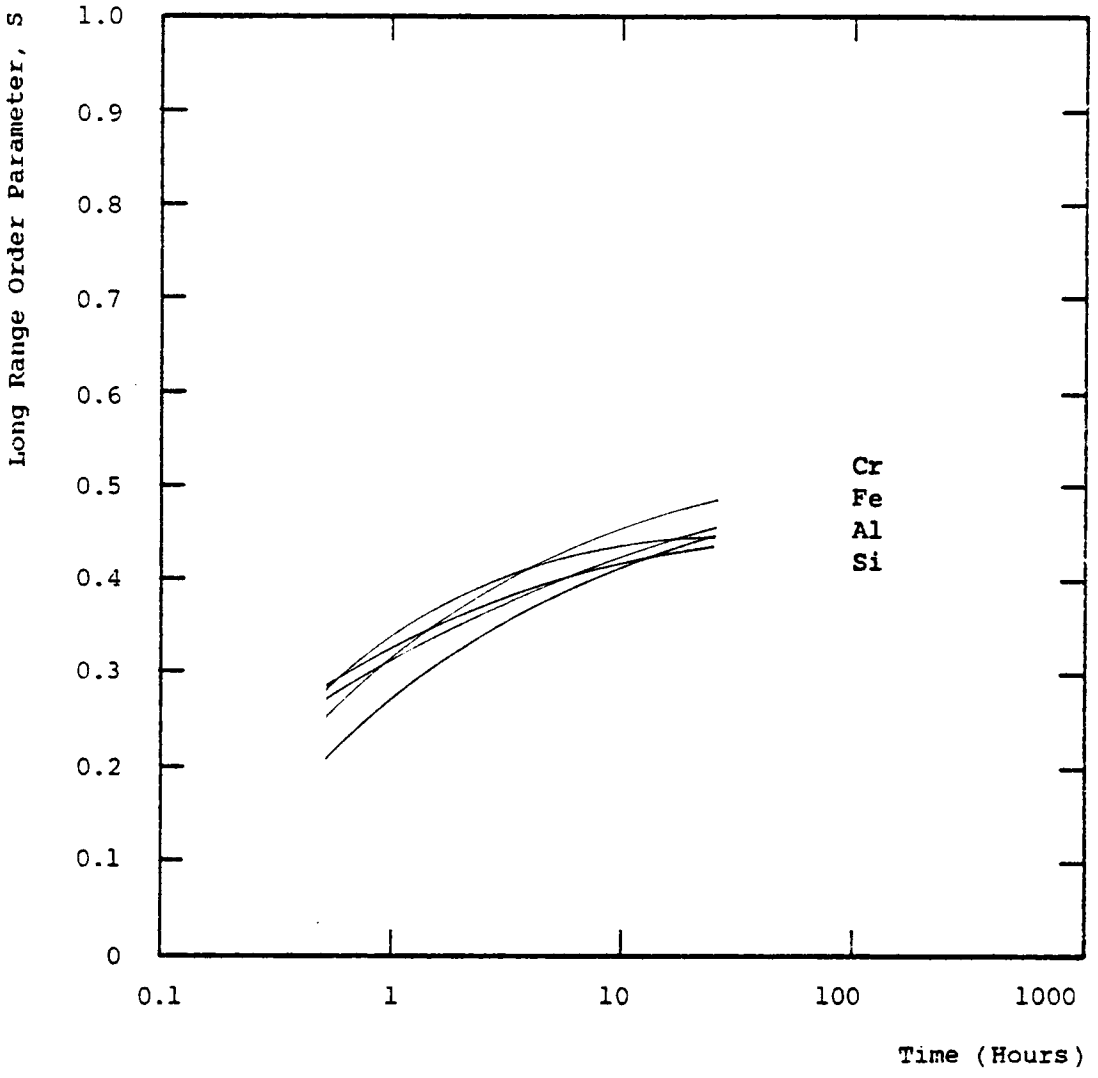


Figure 5.9. Long range order parameter of samples with 0.5 at.% alloy addition, aging temperature 650°C.

additions at 650°C (Fig. 5.9), the Al alloy was probably separable from the other three. None of the others was separable.

For the hardness data showing the effect of 0.5 and 1 at.% additions, Figures A.1-A.12, Appendix, the curves which are separable with a probability of at least 0.9 are drawn separately.

5.3 The Effect of the Amount of Addition

First, the effect of the amount of alloying addition on the degree of ordering will be considered. Graphs of the long range order parameter, S, versus the aging time for each addition at 0.5 and 1 at.% concentrations are shown in Figures 5.1-5.5. At an aging temperature of 700°C, the alloys containing 1 and 0.5 at.% Cr ordered at essentially the same rate. For the aging temperature of 650°C, the 0.5 at.% Cr alloy ordered slightly faster than the 1 at.% Cr alloy (Fig. 5.1). For the alloys with Si additions (Fig. 5.2), there was no difference in the ordering rate of the two alloys at either temperature. The data for the 1 at.% Fe alloy was inconsistent, so, only data for the 0.5 at.% addition is shown (Fig. 5.3). For the alloys with Al additions, the alloy with 1 at.% Al ordered more slowly than the alloy with 0.5 at.% Al at both aging temperatures (Fig. 5.4).

The pure Ni_4Mo (Fig. 5.5) alloy showed a similar or slightly greater degree of order for a given aging time than the other alloys at an aging temperature of 700°C. The slope of the S versus t curve--the ordering rate--for Ni_4Mo at 650 and 700°C is noticeably steeper than the slopes of the other eight curves. At 650°C, the degree of order of

the pure Ni_4Mo alloy is lower than the other alloys for short times, but rises above them as aging proceeds.

In summary, alloying additions tend to decrease the ordering rate of Ni_4Mo, and, as the amount of the addition increases from 0 to 0.5 to 1%, the ordering rate decreases. For the case of the amounts added in this work, the effect is, however, very small.

The hardness data do not always corroborate the x-ray data. Graphs of hardness versus aging time for each addition at 0.5 and 1 at.% concentrations and for each aging temperature are shown in Figures A.1-A.12, Appendix. As mentioned earlier, curves drawn separately in these figures are statistically separable. In the case of the Cr alloys, at an aging temperature of 750°C, the rate of change of the hardness is higher for the 0.5 at.% alloy than for the 1 at.% alloy. At 700°C, the opposite is true. At 650°C, the rate is the same for both alloys although, over the time period considered in this study, the hardness of the 1 at.% alloy is greater than that of the 0.5 at.% alloy.

For the Si alloys, at an aging temperature of 750°C, the rate of change of the hardness and the hardness values of both alloys are the same. At 700°C, the rate of change for the 0.5 at.% alloy is higher, and, at 650°C, the rate of change and the hardness values of both alloys are again very similar.

For the Fe alloys, at the aging temperatures of 750 and 700°C, the rates of change for the two alloys are the same, but the hardness of the 1 at.% alloy is higher. At 650°C, the hardness behavior both alloys is very close.

For the Al alloys, at the three aging temperatures, the hardness behavior of the 0.5 and 1 at.% alloys is very similar.

In summary, for an aging temperature of 750°C, the hardness of the 0.5 at.% Cr alloy is greater than that of the corresponding 1 at.% alloy, the opposite is true for the Fe alloys, and the others are inseparable. At 700°C, the hardness of the 1 at.% Cr, Si, and Fe alloys is greater than that of the corresponding 0.5 at.% alloys. The Al alloys cannot be separated. At 650°C, the hardness of all of the 0.5 at.% alloys is less than or equal to the corresponding 1 at.% alloy.

It is difficult to draw any conclusions about the effect of alloying additions on hardness. The differences in the hardness curves of the 0.5 and the 1 at.% alloys may reflect factors in addition to the increase in hardness associated with the degree of order, such as the variability with temperature and alloy of the rate of formation and disappearance of the network of anti-phase domain boundaries.

5.4 The Effect of the Type of Addition

The effect that each of the four additions to the Ni_4Mo base has on the degree of order will now be considered. Graphs of the long range order parameter, S, versus aging time are shown in Figures 5.6-5.9. (These are the best curves through the data. The data points, which were shown earlier, have been omitted for clarity.) At an aging temperature of 700°C, the elements which, in an addition of 1 at.%, have the least effect on retarding the order are Cr, then Al. Si is the most effective (Fig. 5.6). At 650°C, Si is less effective than Cr or Al; the effect of the latter cannot be distinguished (Fig. 5.7). As mentioned

earlier, the x-ray data for the 1 at.% Fe addition was inconsistent and was hence discarded.

For 0.5 at.% additions, at 700°C, Si and Fe are slightly more effective than Cr and Al (Fig. 5.8). At 650°C, Al has less effect then Cr, Fe, or Si (Fig. 5.9).

This comparison leads to the conclusion that additions of Si and Fe are slightly more effective in retarding ordering than Cr and Al. However, for the amount of third element additions considered here, the difference in ordering rate among the four alloys is minimal, and the decrease in ordering as compared to the pure Ni_4Mo is very small. This agrees with the results of Lei [38] for small Fe additions.

The hardness values are very close (and not necessarily separable) for all of the additions at any given temperature and concentration. The only conclusion which can be drawn from the hardness data is that all four additions have a similar effect on the ordering reaction. Graphs of hardness versus aging time are shown in Figures A.13-A.18, Appendix.

5.5 The Effect of Temperature

The effect of the aging temperature on the rate of ordering will now be discussed. The long range order parameter, S, was calculated for all nine alloys at two temperatures, 700°C and 650°C. After aging at 700°C for 8 h., the alloys with 1 at.% addition had reached a degree of order of ~65%. Aging at 650°C for the same time gave a degree of order of only ~40%. The difference is comparable for the alloys with 0.5 at.% or no additions.

The aging temperature had a comparable effect on the degree of hardness obtained. For the alloys with 1 at.% additions, the average hardness after aging for 24 h. was 425(±10) DPH for an aging temperature of 750°C, 400(±10) DPH for 700°C, and 390(±10) DPH for 650°C. There is similarly a decrease in hardness with decreasing aging temperatures for the alloys with 0.5 at.% additions.

5.6 The Microstructure

The microstructures of the eight alloys were studied after 0.5, 1, 2, 4, 8, 24, and 48 h. aging treatments at 650 and 700°C and after 0.5, 1, 2, 4, 8, and 24 h. aging treatments at 750°C. The initial microstructure associated with the α-phase consists of equiaxed grains, featureless except for annealing twins. Two microstructural changes occurred during the time period considered. First is grain boundary migration and the subsequent formation of new grains at the grain boundary. This phenomenon is probably a recovery and recrystallization process induced by the strain associated with the phase change. Second is the appearance of a striated structure in the former α-phase grains. This structure is associated with the formation of the β-phase.

The aging time required for the microstructural changes to occur is a function of the amount and type of addition, as well as the aging temperature. However, apart from the time required for a given change to occur, it was not possible to distinguish the samples by their microstructure. The microstructural changes will be discussed with reference to a representative selection, 0.5 and 1 at.% Si, shown in Figures 5.10-5.17.

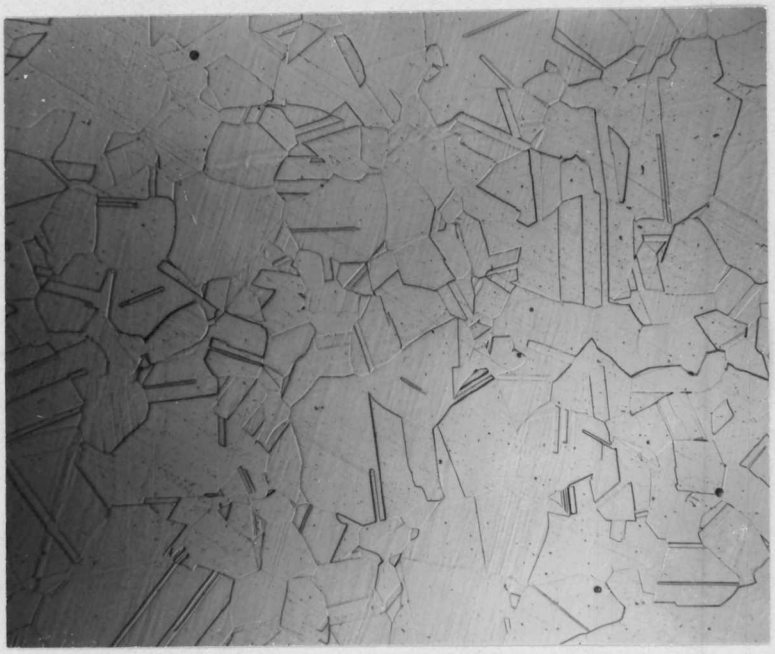


Figure 5.10. The 0.5 at.% Si sample as quenched, 200X.



Figure 5.11. The 0.5 at.% Si sample as quenched, 500X.



Figure 5.12. The 1 at.% Si sample after aging 4 h. at 700°C, 500X.

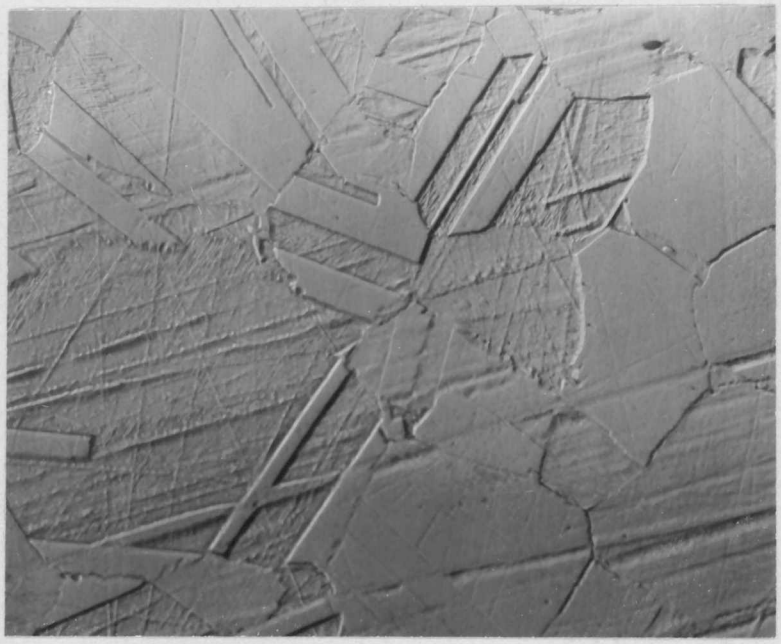


Figure 5.13. The 0.5 at.% Si sample after aging 4 h. at 700°C, 500X.



Figure 5.14. The 1 at.% Si sample after aging 8 h. at 700°C, 500X.



Figure 5.15. The 0.5 at.% Si sample after aging 8 h. at 700°C, 500X.



Figure 5.16. The 1 at.% Si sample after aging 48 h. at 700°C, 500X.



Figure 5.17. The 0.5 at.% Si sample after aging 48 h. at 700°C, 500X.

Figures 5.10 and 5.11 show the 0.5 at.% Si sample as quenched from 1000°C. No changes in the microstructure were seen after 0.5, 1, and 2 h. of aging at 700°C. After 4 h. at 700°C, irregularities had begun to appear at the grain boundaries, and striations had appeared in some grains (Fig. 5.12 and 5.13). After 8 h. at 700°C, the grain boundaries had become slightly more irregular and the striations more extensive (Fig. 5.14 and 5.15). A slight increase in the irregularity of the grain boundaries was noted after 24 h. at 700°C. After 48 h. at 700°C, the grain boundaries of the 1 at.% Si alloy had become very wavy, and a similar reaction was beginning at the twin boundaries. The striated structure was visible in all grains (Fig. 5.16). The 0.5 at.% Si alloy showed a similarly striated structure and, moreover, many new grains at the grain boundaries and former twin boundaries (Fig. 5.17).

The effect of Si, Cr, Al, and Fe additions on the aging time at 700°C required to produce these two microstructural changes will now be considered. The Si alloys were the first to show any change. Grain boundary irregularities and slight striations in the grain surface appeared after 4 h. No changes were visible in the other alloys after 4 h.

After 8 h., a slight waviness appeared in the grain boundaries of the 0.5 at.% Cr, Al, and Fe alloys. Striations became visible in some of the grains. No changes were noted in the grain boundaries of the 1 at.% Cr, Al, or Fe alloys, although all exhibited some striations.

After 24 h., new grains appeared at the grain boundaries of the 0.5 at.% Si and Al alloys. The grain boundaries of the 1 at.% Cr, Al, and Fe alloys became slightly irregular.

After 48 h., new grains appeared near the grain boundaries of the 0.5 at.% Cr and Fe alloys. At this point, the appearance of the 0.5 and 1 at.% alloys was quite different, as can be seen by comparing Figures 5.16 and 5.17.

The appearance of the microstructures of the eight alloys while aging at 750°C was comparable to the appearance while aging at 700°C although the changes occurred after a shorter aging time. New grains appeared after 24 h. in the 0.5 at.% Si, Cr, and Al alloys. Likewise, the microstructures of the samples aged at 650°C were similar although a longer aging time was required for a given change to occur.

The aging time required for a given microstructural change to occur is a function of the amount and type of third element addition and of the aging temperature. Changes occurred most rapidly in the alloys with the 0.5 at.% addition. The changes were noted in the Si alloys after the shortest aging times, then the Al alloys, then the Cr alloys. The Fe alloys required the longest aging treatment for a given change to occur. As for the LRO parameter and the hardness, the microstructural changes were most rapid at 750°C and slowest at 650°C.

The onset of grain boundary migration and the subsequent recrystallization may be directly indicative of the degree of order attained or may be a function of the ability of each alloy to accommodate the strain induced by the phase change. The latter may be the case here because the samples containing Si and Al were the first to recrystallize, and, as was mentioned in Section 3.4, the atomic radii of Si and Al differ significantly from those of Ni and Mo. This implies that the initial lattice strain is higher than for the alloys with Cr and Fe. If

this is indeed the case, the onset of grain boundary migration and recrystallization cannot be directly correlated with the extent of the phase change but can be used as a measure of atomic misfit, which may be an important criterion in choosing an addition to retard ordering.

It is not possible to correlate the microstructural changes with the hardness and LRO parameter behavior without data for longer times. Recrystallization, one of the processes which would be expected to have a significant effect on the hardness, is just beginning at the longest aging time studied.

6. CONCLUSIONS AND RECOMMENDATIONS

Third element additions to Ni_4Mo were found to decrease the ordering rate at the temperatures studied, 650 and 700°C. Increasing the amount of the addition from 0.5 to 1 at.% caused a decrease in the ordering rate. Si and Fe appeared to have slightly more effect than Cr or Al. For the three aging temperatures considered in this study, ordering was fastest at the highest temperature, 750°C, and slowest at 650°C, the lowest temperature studied.

Two processes were revealed by the microstructural study. The $\alpha \rightarrow \beta$ phase change was evidenced by the appearance of a striated structure associated with the β-phase. A reaction involving grain boundary migration followed by recrystallization was also seen in all of the samples. At 750, 700, and 650°C, the process first took place in the samples containing Si, then Al, and then Cr and Fe. It was concluded that this process occurred because of strain induced during the $\alpha \rightarrow \beta$ phase change.

There are several aspects of this subject which deserve further study. Specifically, the effect of larger additions of Cr, Si, Fe, and Al to Ni_4Mo on the order parameter should be investigated. It is reasonable to assume that additions of these elements in sufficient amounts will suppress the ordering reaction. The mechanical and corrosion behavior of these alloys should then be studied. More generally, knowledge about the manner in which an addition slows or stops the ordering reaction in Ni_4Mo would be useful. This includes information about the lattice site which an addition occupies and about the effect that the addition has on the phase relations, the change in the lattice

parameter as ordering proceeds, the formation and growth of anti-phase domains, and the diffusion rates of the components. Such results could then be used to predict the most effective addition.

REFERENCES

REFERENCES

[1] Artsishevskaya, L. F., I. B. Malysheva, Ya. P. Selisshiy. An investigation of ordering kinetics in Ni-Mo alloys. Phys. Met. Met., V. 33, pp. 144-148, 1972.

[2] Bain, E. C. The nature of solid solutions. Chem. and Met. Eng., V. 28, pp. 21-24, 1923.

[3] Bain, E. C. Cored crystals and metallic compounds. Chem. and Met. Eng., V. 28, pp. 65-69, 1923.

[4] Bain, E. C. Crystal structure of solid solutions. Trans. AIME, V. 68, pp. 625-639, 1923.

[5] Barrett, C. S. Structure of Metals, Second Edition. McGraw-Hill Co., New York, 1952.

[6] Bethe, H. A., H. H. Wills. Statistical theory of superlattices. Proc. Royal Soc., V. A150, pp. 552-575, 1935.

[7] Bloom, D. S., N. J. Grant. An investigation of the systems formed by Cr, Mo, and Ni. Trans. AIME, V. 200, pp. 261-268, 1954.

[8] Bragg, W. L., E. J. Williams. The effect of thermal agitation on atomic arrangement in alloys. Proc. Royal Soc., V. A145, pp. 699-730, 1934.

[9] Casselton, R. E. W., W. Hume-Rothery. The equilibrium diagram of the system Mo-Ni. J. of the Less Common Metals, V. 7, pp. 212-221, 1964.

[10] Chakravarti, B., E. A. Starke, Jr., B. G. LeFevre. Order-induced strengthening in Ni_4Mo. J. Mat. Sci., V. 5, pp. 394-406, 1970.

[11] Chakravarti, B., E. A. Starke. Jr., C. J. Sparks, R. O. Williams. Short range order and the development of long range order in Ni_4Mo. J. Phys. and Chem. of Solids, V. 35, pp. 1317-1326, 1974.

[12] Chevalier, J. P., W. M. Stobbs. An electron diffraction study of short range order in quenched Ni_4Mo alloy. Acta Met., V. 24, pp. 535-542, 1976.

[13] Chevalier, J. P., W. M. Stobbs. Quenched and aged Ni_4Mo, in Developments in Electron Microscopy and Analysis. J. A. Venables, Ed., Academic Press, New York, 1976.

[14] Christian, J. W. The Theory of Transformations in Metals and Alloys. Pergamon Press, New York, 1965.

[15] Clapp, P. C., S. C. Moss. Correlation functions of disordered binary alloys, II. Phys. Rev., V. 171, pp. 754-763, 1968.

[16] Cohen, J. B. A brief review of the properties of ordered alloys. J. Mat. Sci., V. 4, pp. 1012-1022, 1969.

[17] Das, D. K., S. P. Rideout, P. A. Beck. Intermediate phases in the Mo-Fe-Co, Mo-Fe-Ni, and Mo-Ni-Co ternary systems. Trans. AIME, V. 194, pp. 1071-1075, 1952.

[18] Das, S. K., P. R. Okamoto, P. M. J. Fisher, G. Thomas. Short range order in Ni-Mo, Au-Cr, Au-V, and Au-Mn alloys. Acta Met., V. 21, pp. 913-928, 1973.

[19] DeRidder, R., G. Van Tendeloo, S. Amelinckx. A cluster model for the transition from the short range ordered to the long range ordered state in FCC based binary systems and its study by means of electron diffraction. Acta Cryst., V. A32, pp. 216-224, 1976.

[20] Ellinger, F. H. The Ni-Mo system. Trans. ASM, V. 30, pp. 607-637, 1942.

[21] Elliot, R. P. Constitution of Binary Alloys, First Supplement. McGraw-Hill Co., New York, 1965.

[22] Giamei, A. F., E. J. Freise. Optimization of x-ray diffraction quantitative analysis. Trans. AIME, V. 239, pp. 1676-1685, 1967.

[23] Green, H. S., C. A. Hurst. Order-Disorder Phenomena. John Wiley & Sons, New York, 1964.

[24] Grube, G., H. Schlect. Elektrische Leitfähigkeit und Zustandsdiagram von binären Legierungen des Systems Nickel-Molybdän. Z. Elektrochem., V. 44, pp. 413-422, 1938.

[25] Grube, G., O. Winkler. Magnetische Suszeptibilität und Zustandsdiagram von binären Legierungen des Systems Nickel-Molybdän. Z. Elektrochem., V. 44, pp. 423-428, 1938.

[26] Guthrie, P. V., E. E. Stansbury. X-ray and metallographic study of the Ni-rich alloys of the Ni-Mo system, II. ORNL Report 3078, 1961.

[27] Hansen, M. Constitution of Binary Alloys. McGraw-Hill Co., New York, 1958.

[28] Harker, D. The crystal structure of Ni_4Mo. J. Chem. Phys., V. 12. pp. 315-317, 1944.

[29] Harker, D. Order hardening: Its mechanism and recognition. Trans. ASM, V. 32, pp. 210-234, 1944.

[30] Internationale Tabellen zur Bestimmung von Kristallstrukturen V. 1, Gruppentheoretische Tafeln. Gebrüder Borntraeger, Berlin, 1944.

[31] Kiriyenko, V. J., E. E. Poplavskaya, L. P. Potapov. Influence of alloying elements on ordering in Ni-Mo alloys. Phys. Met. Met., V. 33, pp. 132-138, 1972.

[32] Kiriyenko, V. J., L. P. Potapov. Mechanism of the initial stage of ordering in Ni-Mo alloys. Phys. Met. Met., V. 33, pp. 207-211, 1972.

[33] Kiriyenko, V. J., L. P. Potapov. Investigation of short range order in Ni-Mo alloys. Phys. Met. Met., V. 36, pp. 417-420, 1973.

[34] Kozlov, E. V., V. M. Kushnavenko. Crystallographic x-ray analysis of the order-disorder phase transition in the alloy Ni_4Mo. Phys. Met. Met., V. 46, pp. 75-80, 1978.

[35] Krivoglaz, M. A., A. A. Smirnov. The Theory of Order-Disorder in Alloys, American Elsevier Publishing Co., New York, 1964.

[36] LeFevre, B. G., A. G. Grey, R. W. Gould. Ordering and the K state in Ni-Mo alloys. Trans. AIME, V. 242, pp. 788-795, 1968.

[37] LeFevre, B. G., E. A. Starke, Jr. Changes in the Bragg-Williams parameter with deformation in ordered Au_4V. Advances in X-Ray Analysis, V. 12, Plenum Press, New York, pp. 113-128, 1969.

[38] Lei, T. S. The Effect of 0-8 Weight Percent Iron on Transformations of α Phase Ni-Mo-Fe Alloys with Ni:Mo Ratio Equal to 4:1. PhD. Dissertation, University of Tennessee, 1979.

[39] Ling, F. W., E. A. Starke, Jr. The development of long range order and the resulting strengthening effects in Ni_4Mo. Acta Met., V. 19, pp. 759-768, 1971.

[40] Ling, F. W., E. A. Starke, Jr. The disorder-order transition in Ni_4Mo. Advances in X-Ray Analysis, V. 15, Plenum Press, New York, pp. 319-329, 1972.

[41] Moss, S. C., P. C. Clapp. Correlation functions of disordered binary alloys, III. Phys. Rev., V. 171, pp. 764-777, 1968.

[42] Newman, R. W., J. J. Hren. Field ion microscopy of Ni-Mo alloys. Phil. Mag., Eighth series, V. 16, pp. 211-214, 1967.

[43] Nix, F. C. Superstructures in alloy systems. J. Applied Phys., V. 8, pp. 783-794, 1937.

[44] Norem, W. E. An Investigation of Nickel-Rich Alloys Containing Mo and Fe. M. S. Thesis, University of Tennessee, 1963.

[45] Okamoto, P. R., G. Thomas. On short range order and microdomains in the Ni_4Mo system. Acta Met., V. 19, pp. 825-841, 1971.

[46] Potapov, L. P., A. F. Yedneral, V. J. Kiriyenko, Ye. A. Nikandrova. Structure transitions in Ni-Mo-W alloys. Phys. Met. Met., V. 42, pp. 76-83, 1976.

[47] Rideout, S., W. D. Manly, E. L. Kamen, B. S. Lement, P. A. Beck. Intermediate phases in ternary alloy systems of transition elements. Trans. AIME, V. 191, pp. 872-876, 1951.

[48] Ruedl, E., P. Delavignette, S. Amelinckx. Electron diffraction and electron microscope study of long and short range order in Ni_4Mo and of the substructure resulting from ordering. Physica Status Solidi, V. 28, pp. 305-328, 1968.

[49] Saburi, I., K. Komatsu, S. Nenno. Transition from short range to long range order in Ni_4Mo. Phil. Mag., Eighth series, V. 20, pp. 1091-1094, 1969.

[50] Saburi, I., K. Komatsu, M. Yamamoto, S. Nenno, Y. Mizutani. A new metastable phase Ni_2Mo. Trans. AIME, V. 245, pp. 2348-2349, 1969.

[51] Spruiell, J. E., E. E. Stansbury. X-ray study of short range order in Ni alloys containing 10.7 and 20.0 atomic percent Mo. J. Phys. Chem. Solids, V. 26, pp. 811-822, 1965.

[52] Stoloff, N. S., R. G. Davies. The mechanical properties of ordered alloys. Progress in Materials Science, V. 13, 1966.

[53] Tammann, G. Die chemischen und galvanischen Eigenschaften von Mischkristallreihen und ihre Atomverteilung. Z. Anorg. Chem., V. 107, pp. 1-239, 1919.

[54] Thomas, G., R. Sinclair. Discussion of 'An electron diffraction study of short range order in quenched Ni_4Mo alloy'. Acta Met., V. 25, pp. 231-234, 1977.

[55] Van Tendeloo, G. Short range order considerations and development of long range order in different Ni-Mo alloys. Mat. Sci. and Eng., V. 26, pp. 209-220, 1976.

[56] Warlimont, H., Editor. Order-Disorder Transformations in Alloys, Springer-Verlag, Berlin, 1974.

[57] Warren, B. E. X-Ray Diffraction, Addison-Wesley Publishing Co., Reading, Ma., 1969.

APPENDIX

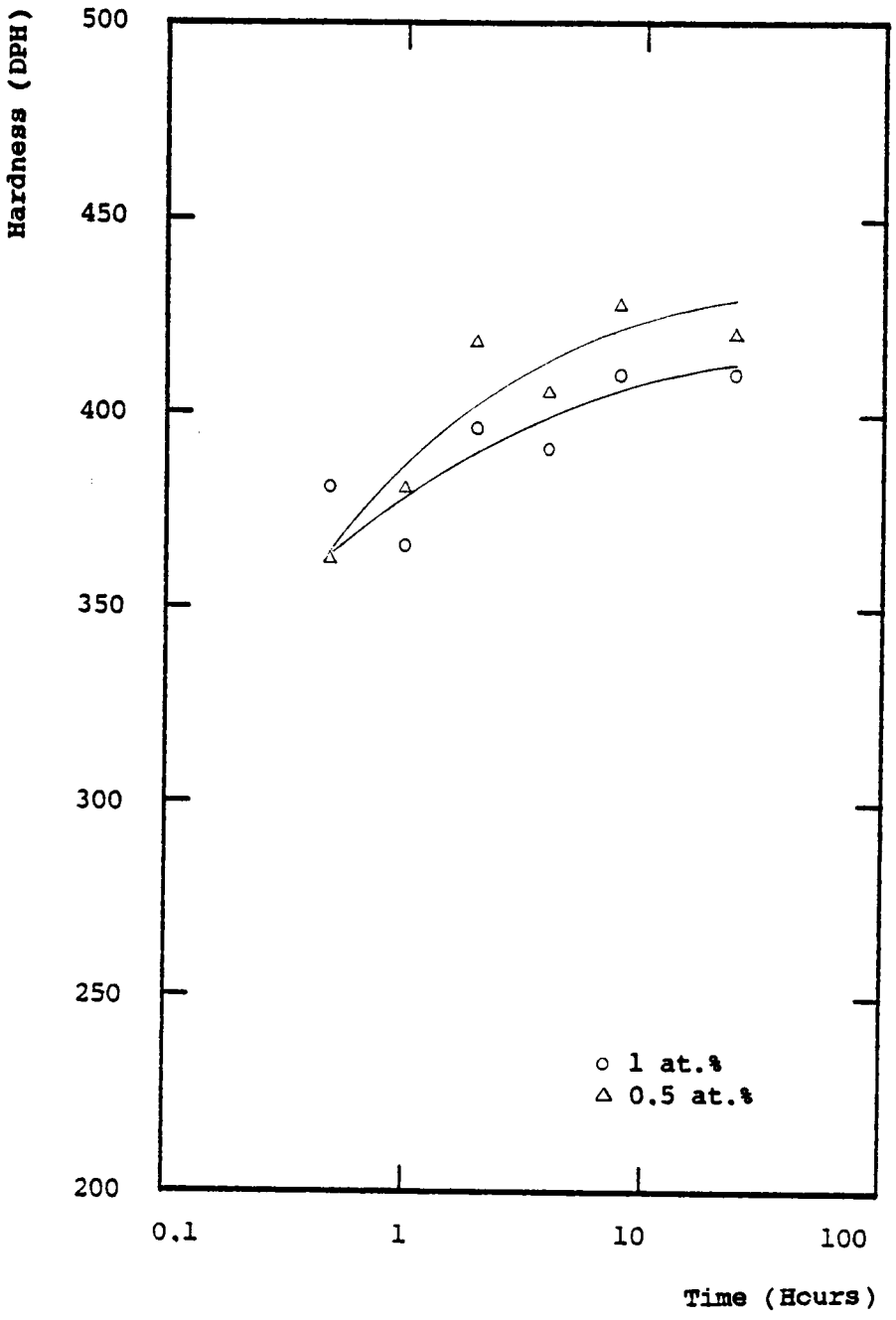


Figure A.1. Hardness of samples with Cr addition, aging temperature 750°C.

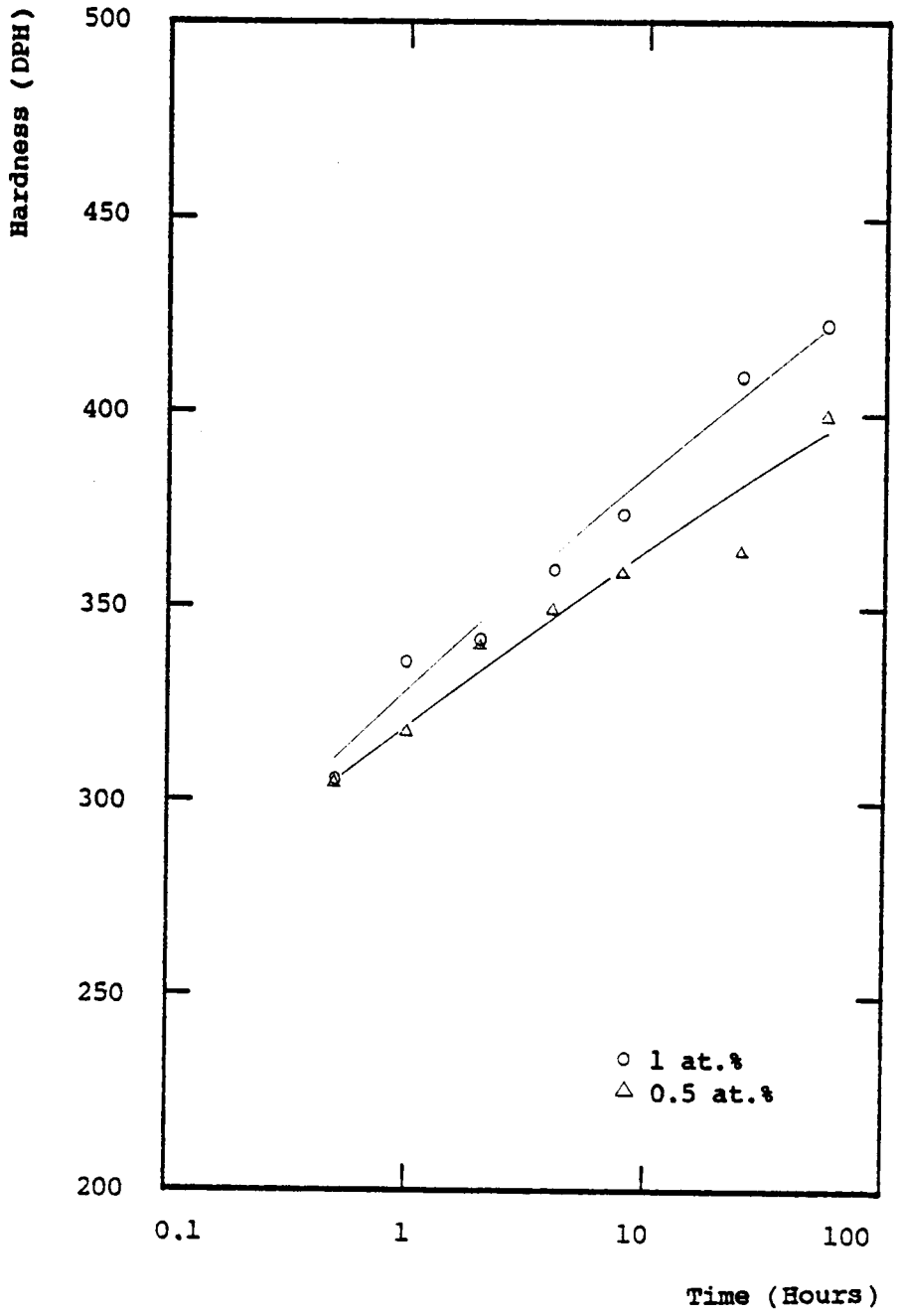


Figure A.2. Hardness of samples with Cr addition, aging temperature 700°C.

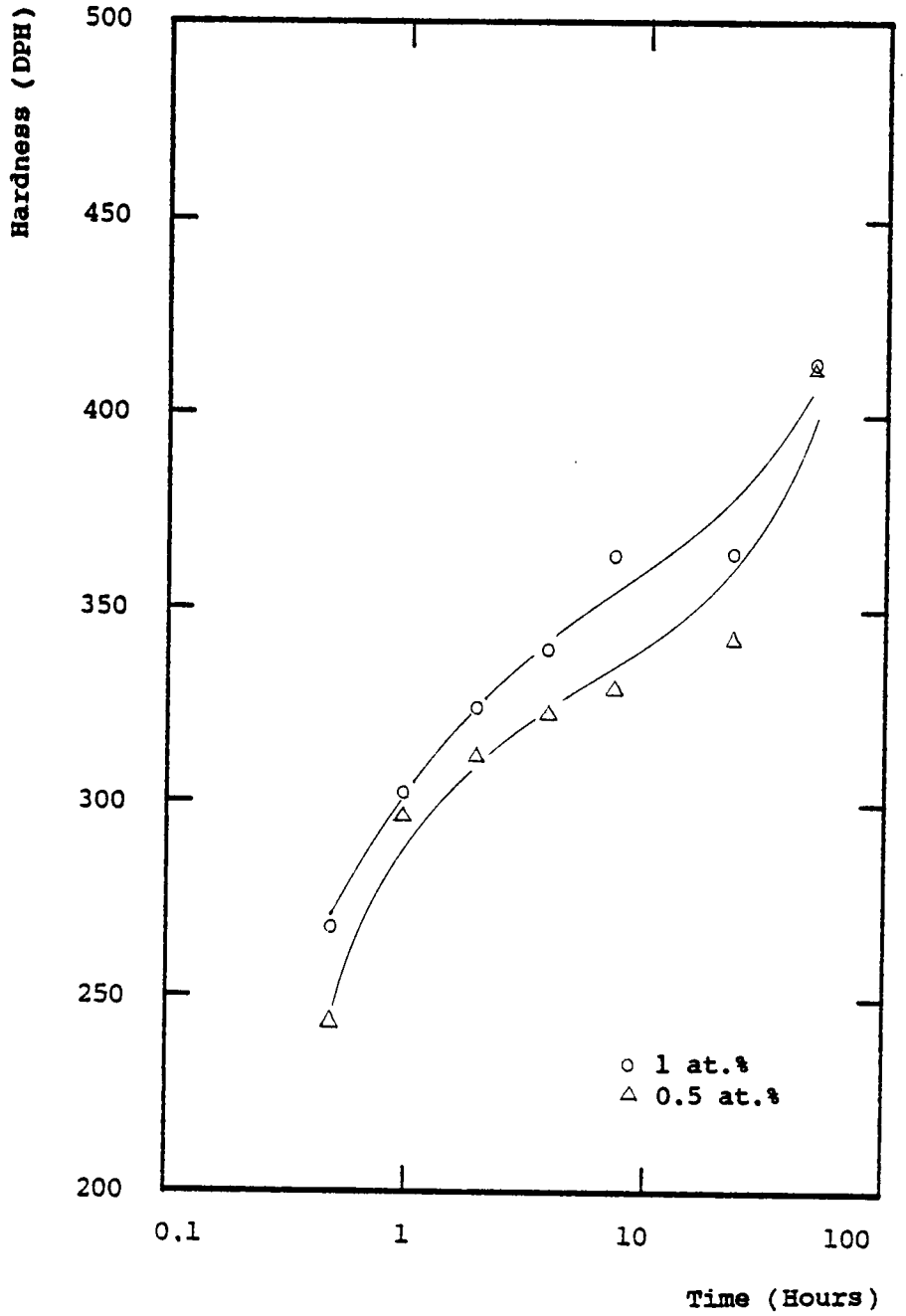


Figure A.3. Hardness of samples with Cr addition, aging temperature 650°C.

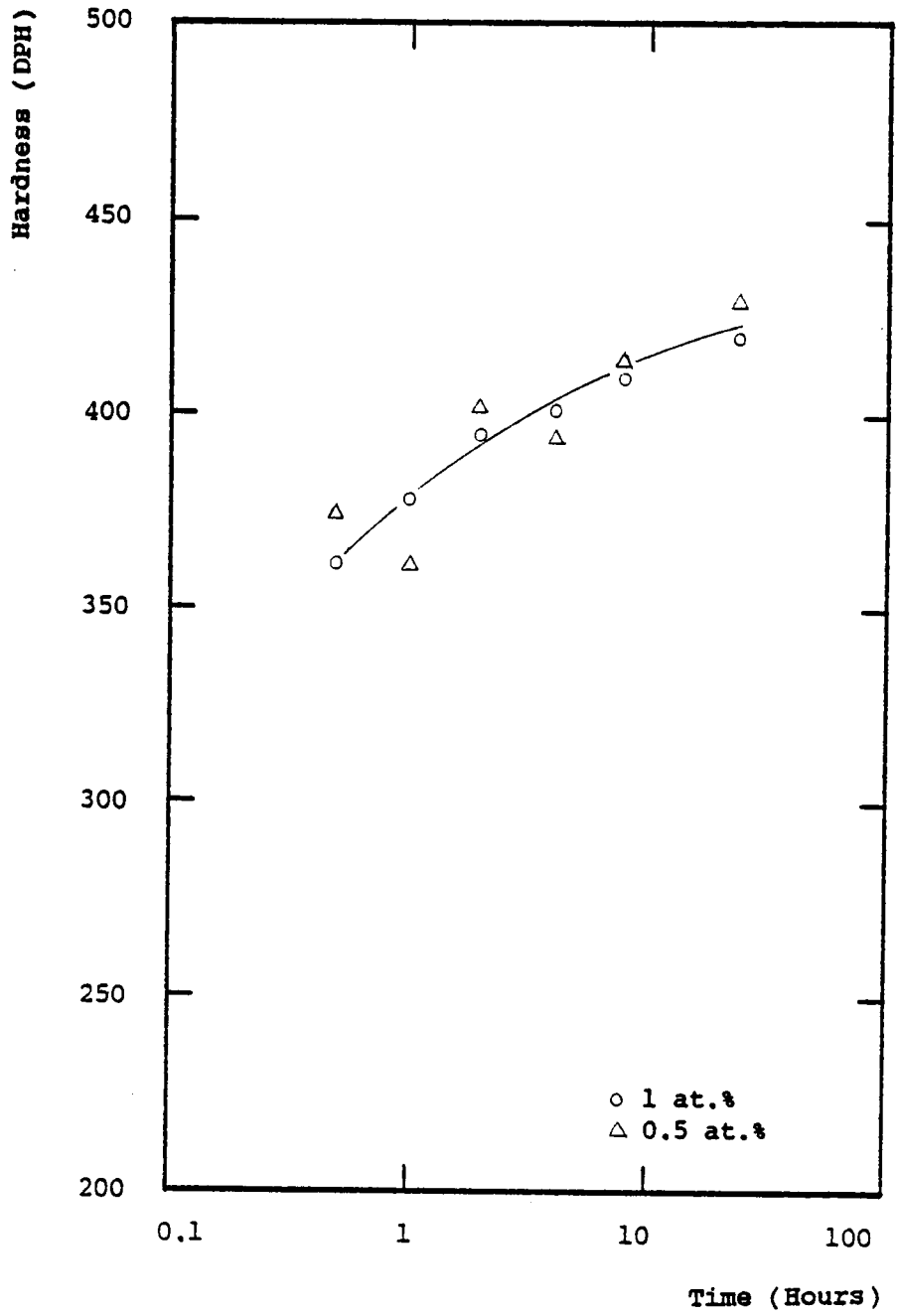


Figure A.4. Hardness of samples with Si addition, aging temperature 750°C.

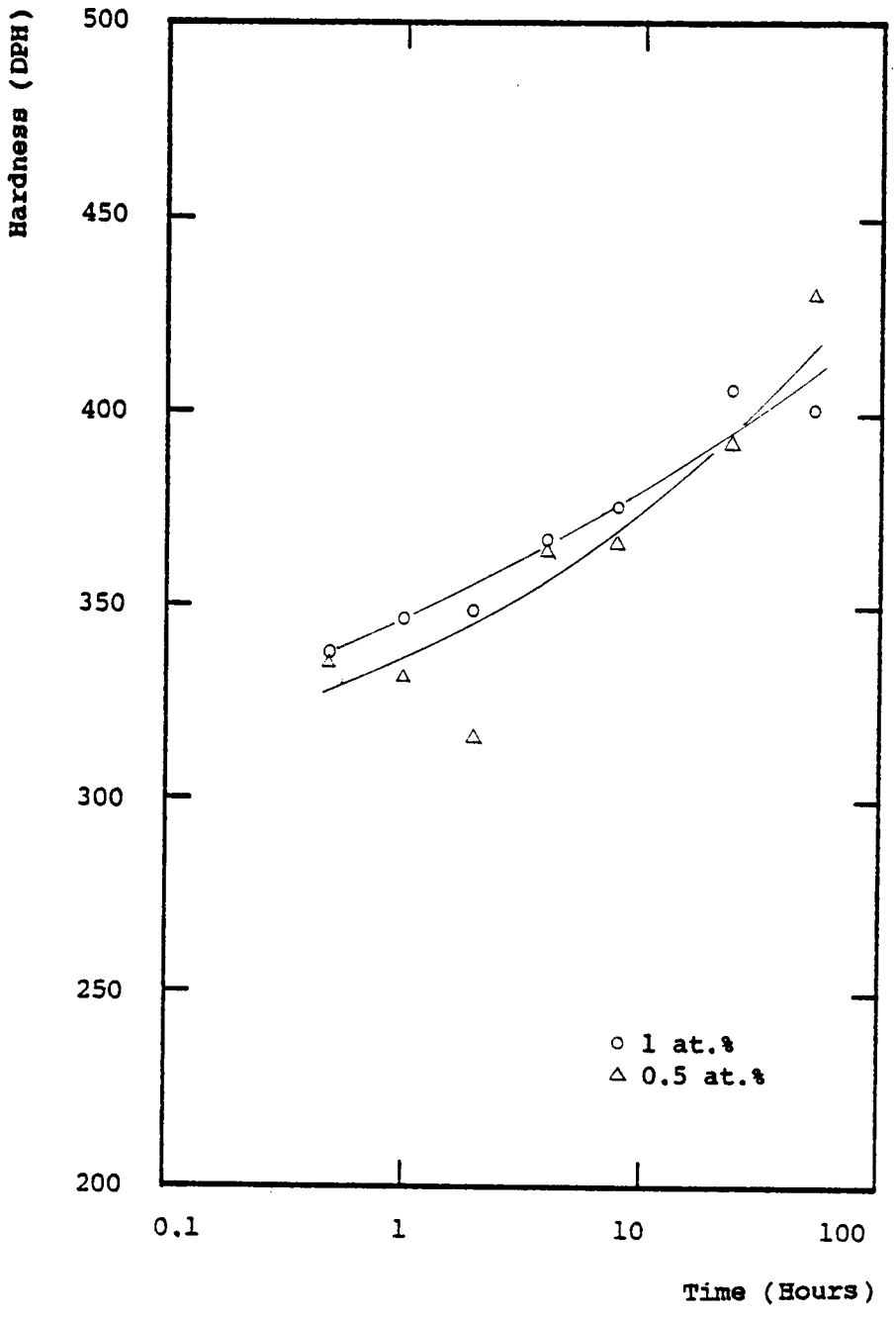


Figure A.5. Hardness of samples with Si addition, aging temperature 700°C.

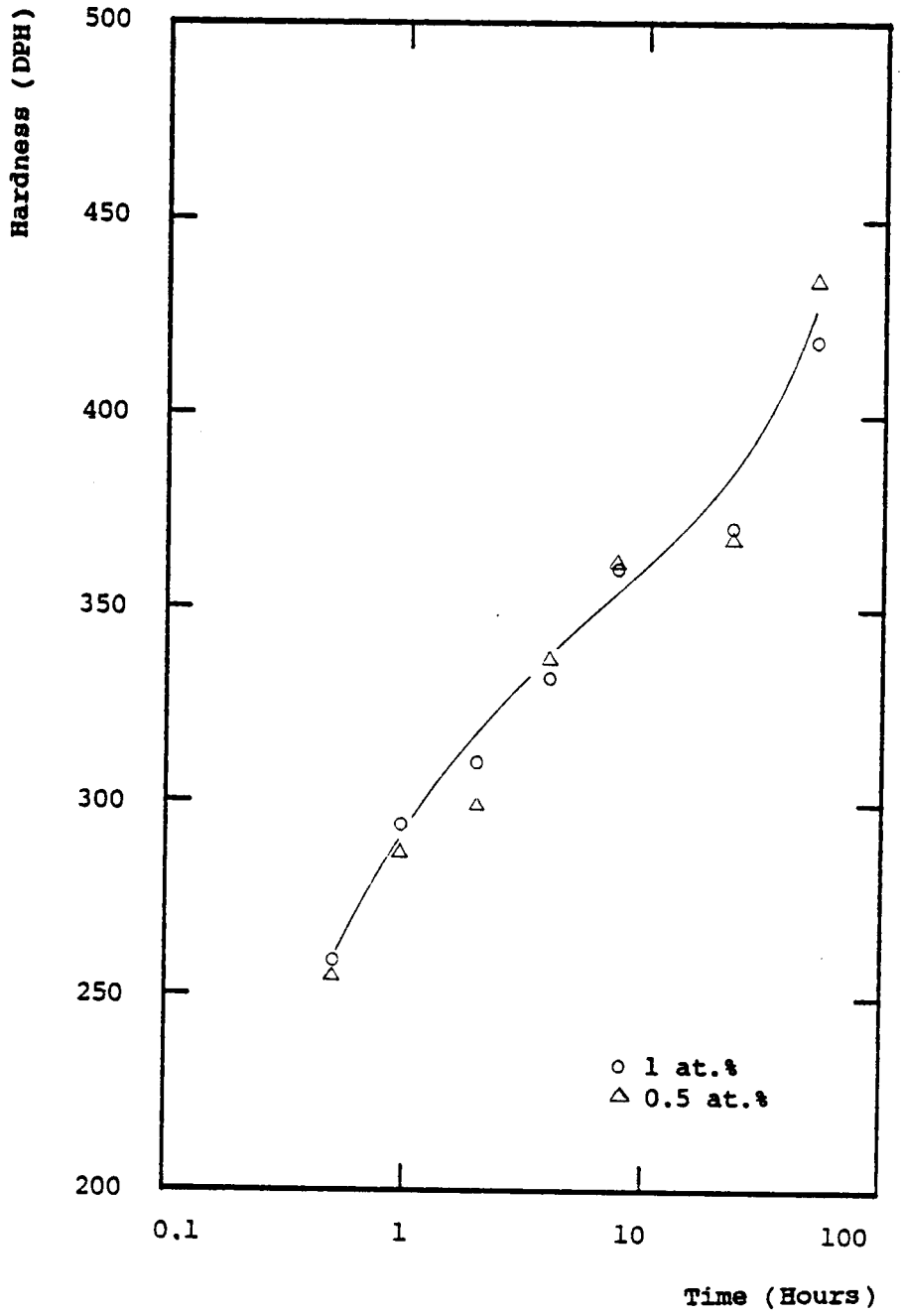


Figure A.6. Hardness of samples with Si addition, aging temperature 650°C.

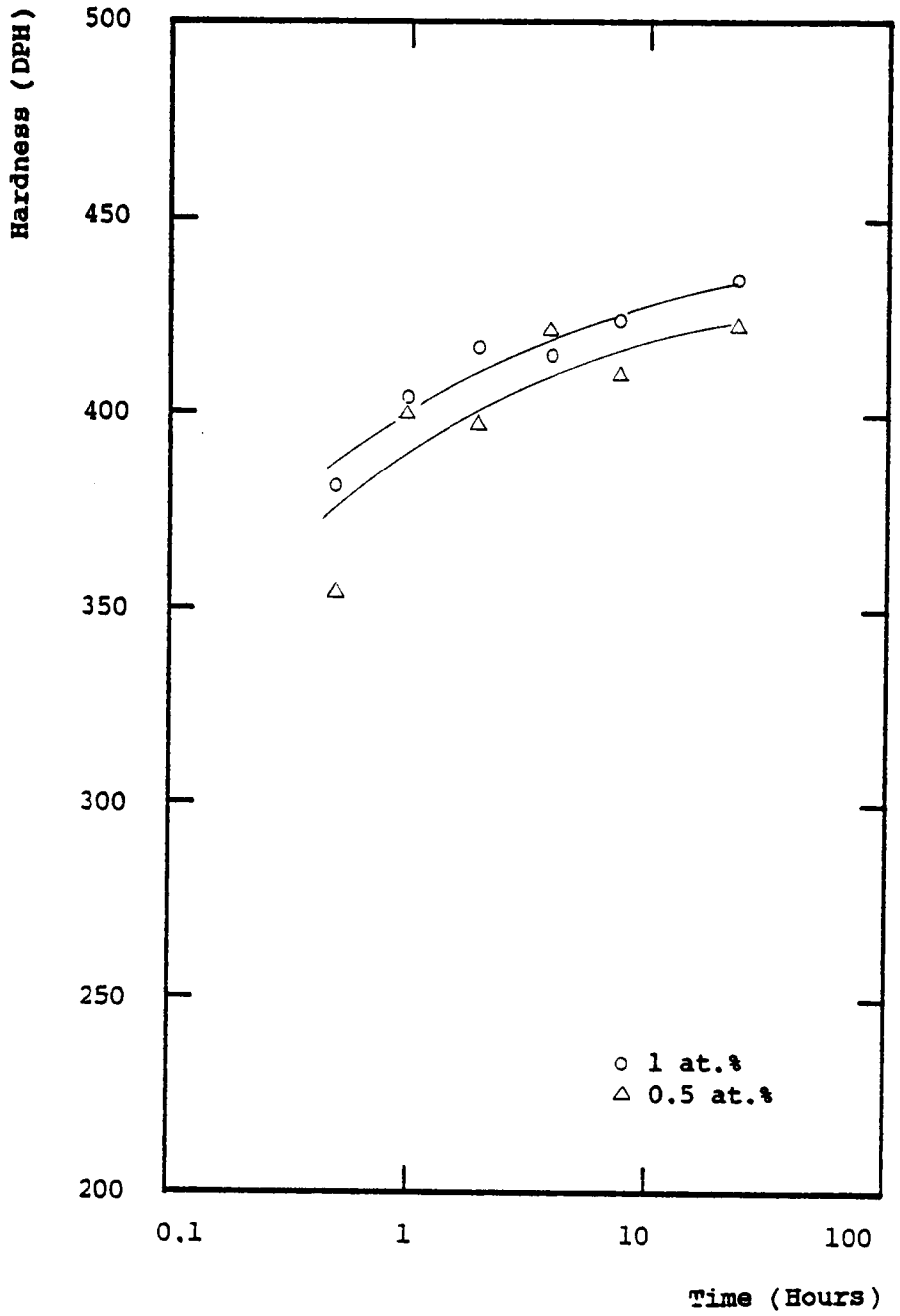


Figure A.7. Hardness of samples with Fe addition, aging temperature 750°C.

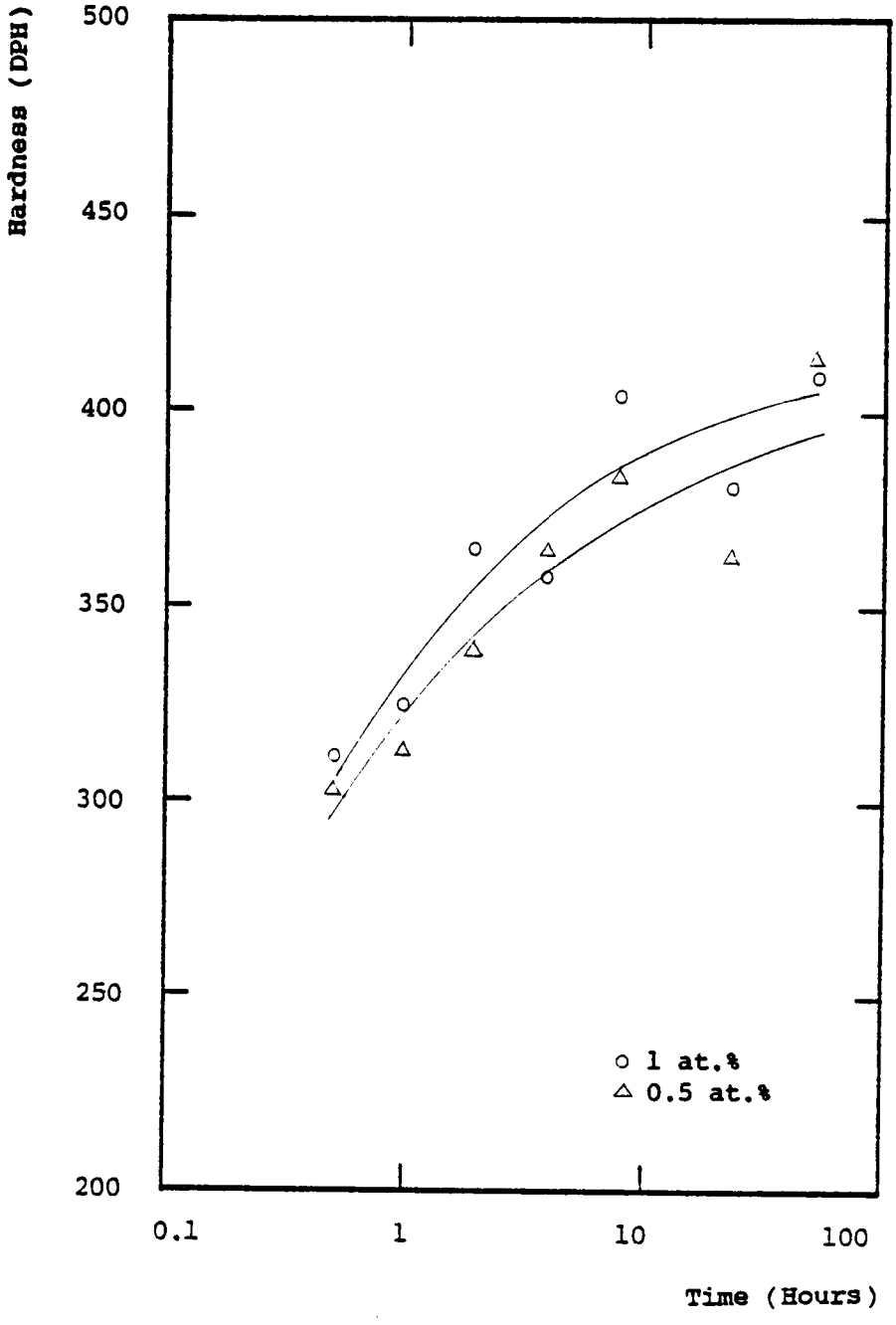


Figure A.8. Hardness of samples with Fe addition, aging temperature 700°C.

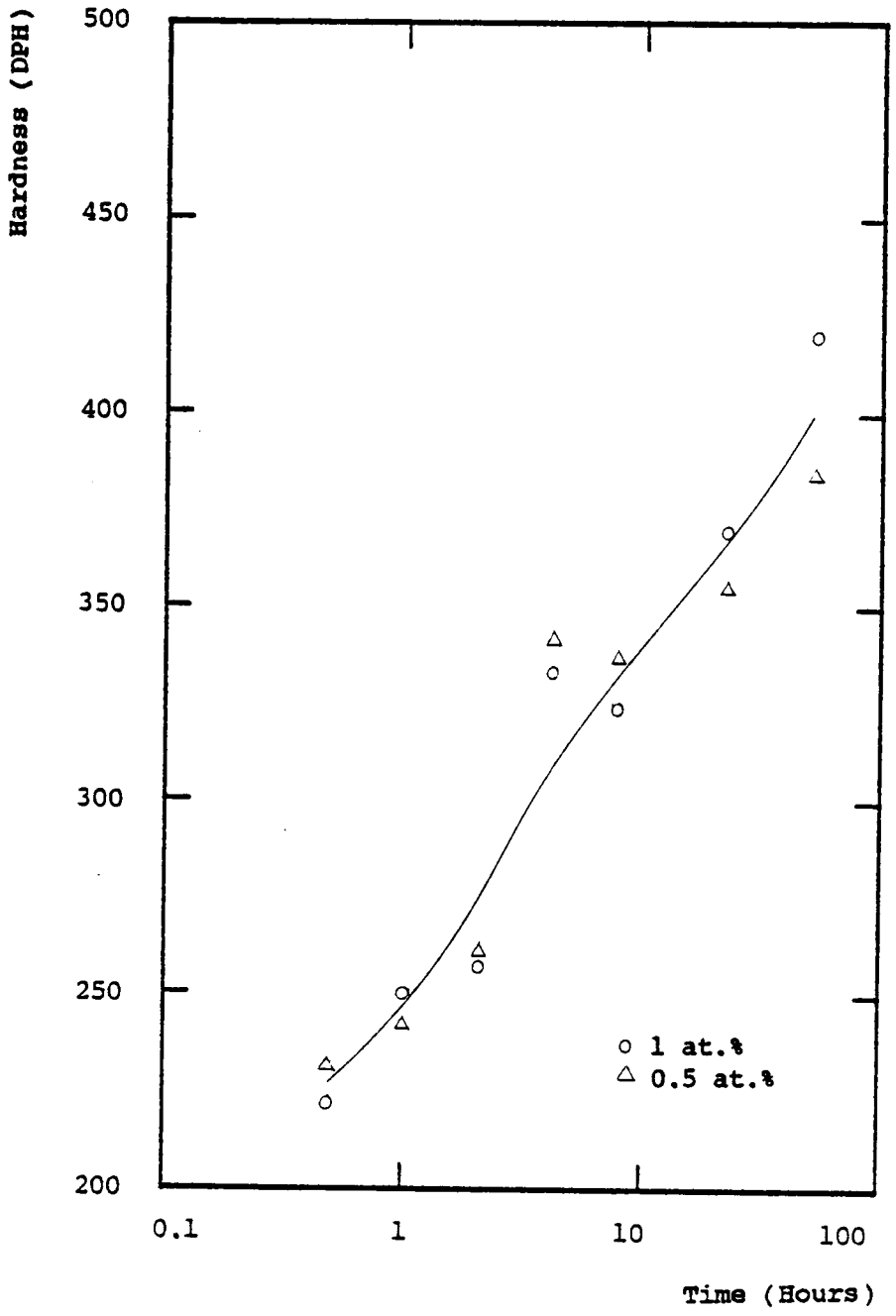


Figure A.9. Hardness of samples with Fe addition, aging temperature 650°C.

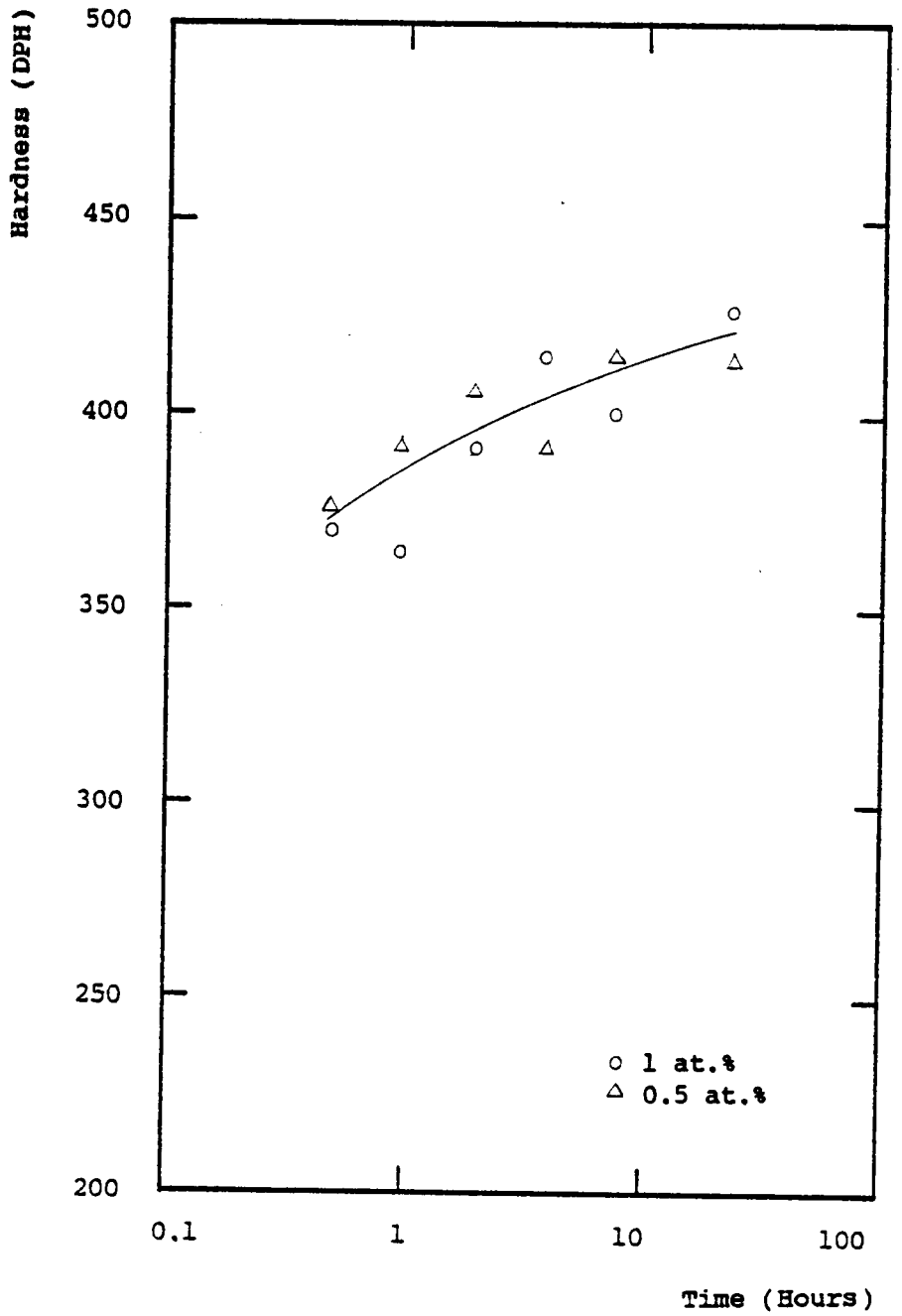


Figure A.10. Hardness of samples with Al addition, aging temperature 750°C.

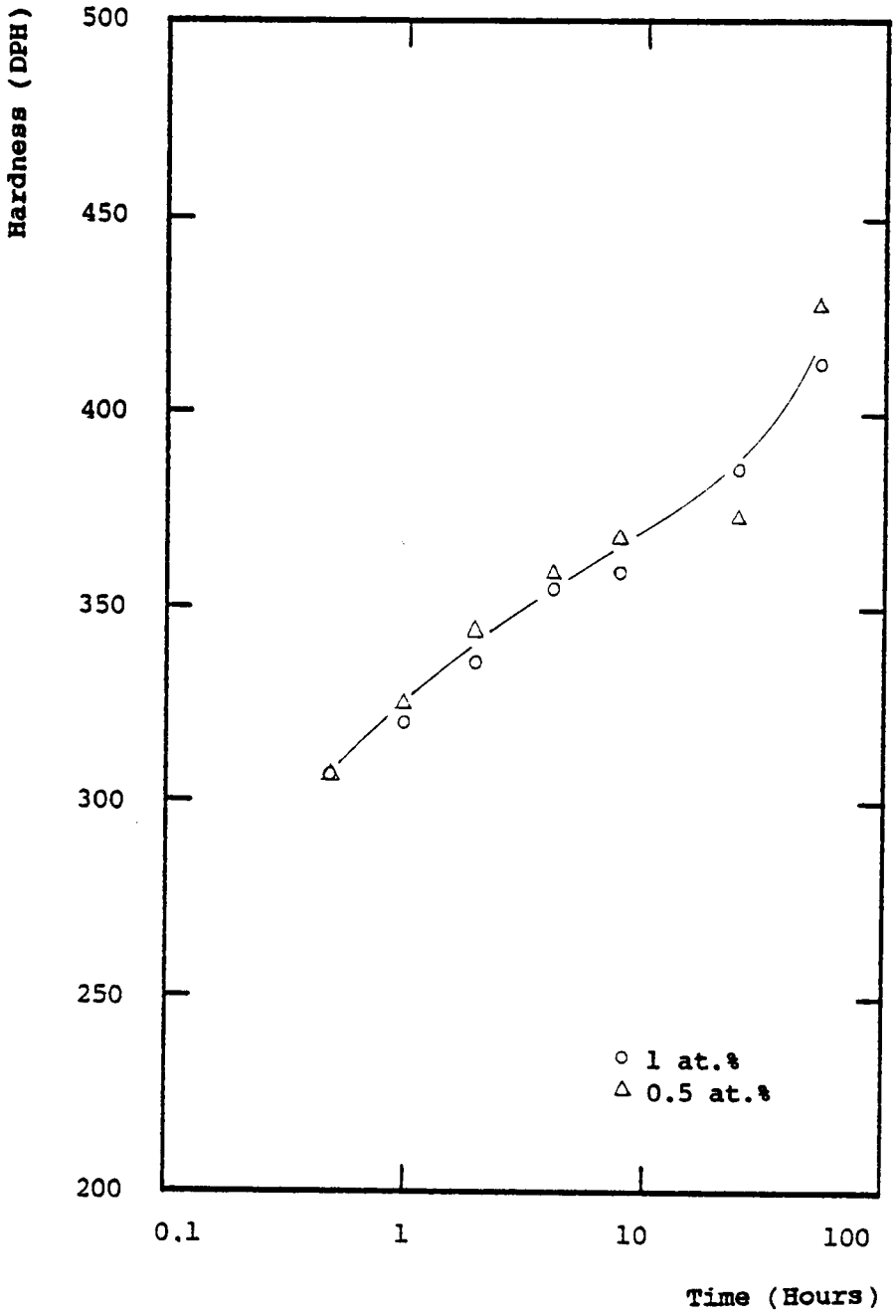


Figure A.11. Hardness of samples with Al addition, aging temperature 700°C.

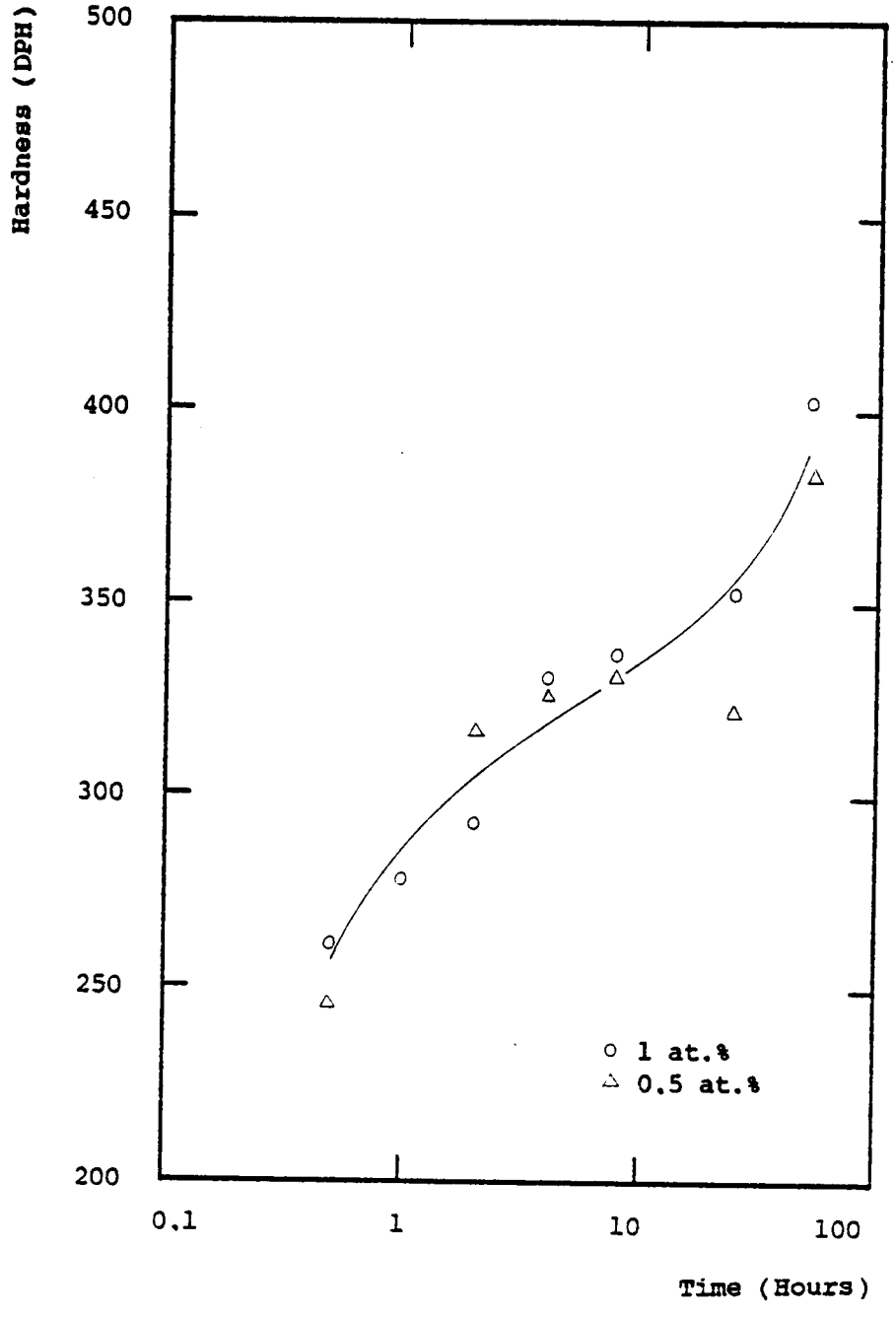


Figure A.12. Hardness of samples with Al addition, aging temperature 650°C.

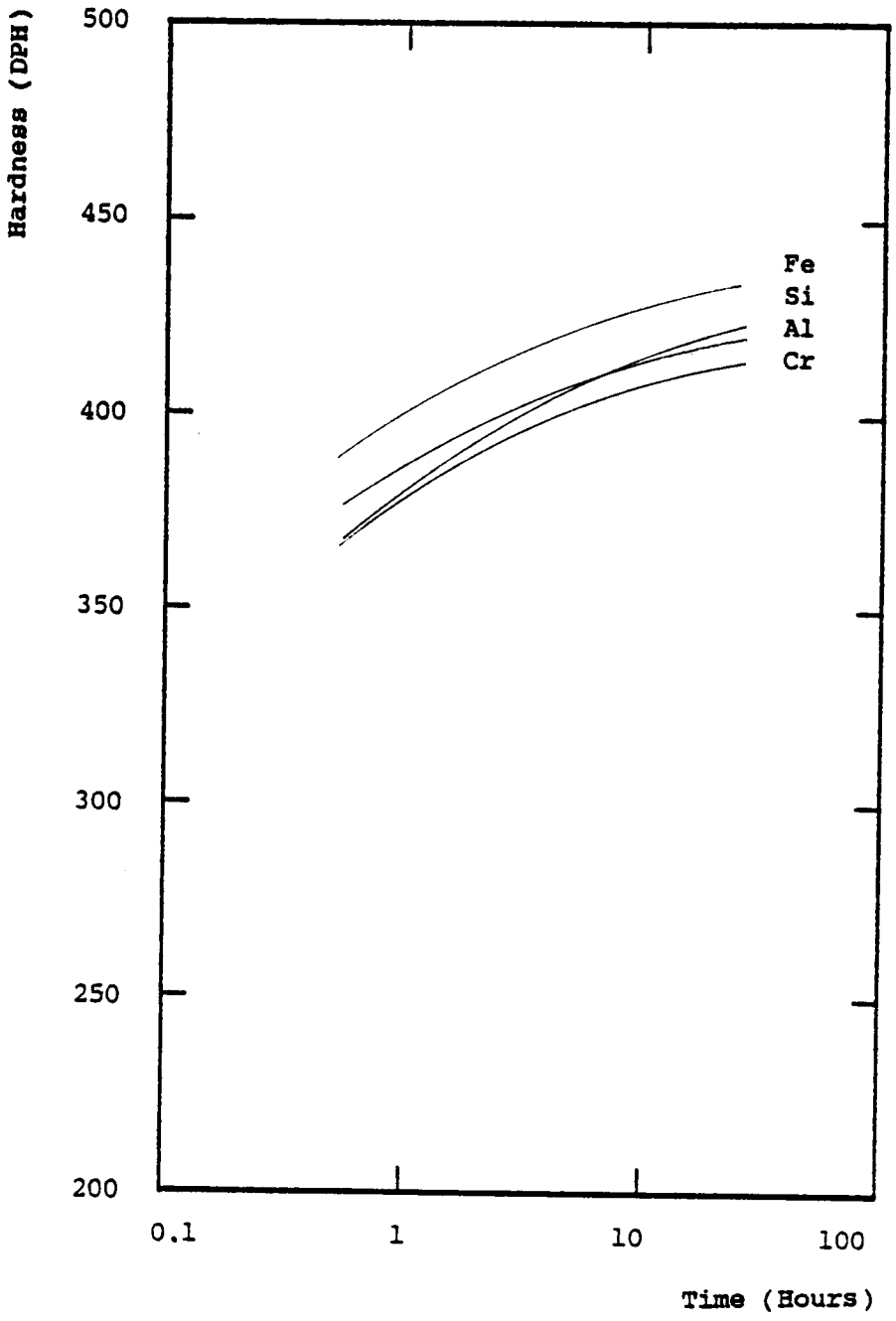


Figure A.13. Hardness of samples with 1 at.% alloy addition, aging temperature 750°C.

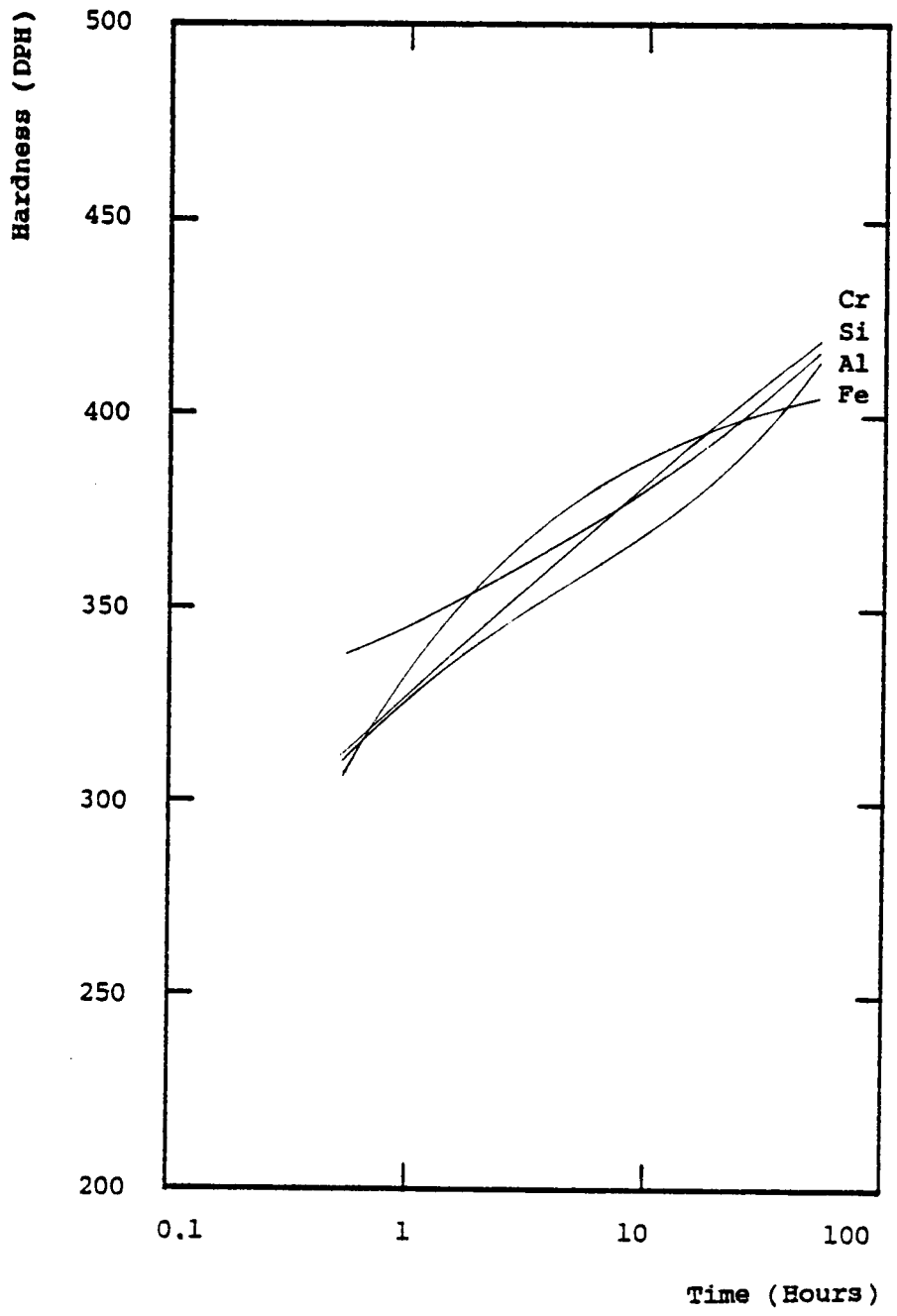


Figure A.14. Hardness of samples with 1 at.% alloy addition, aging temperature 700°C.

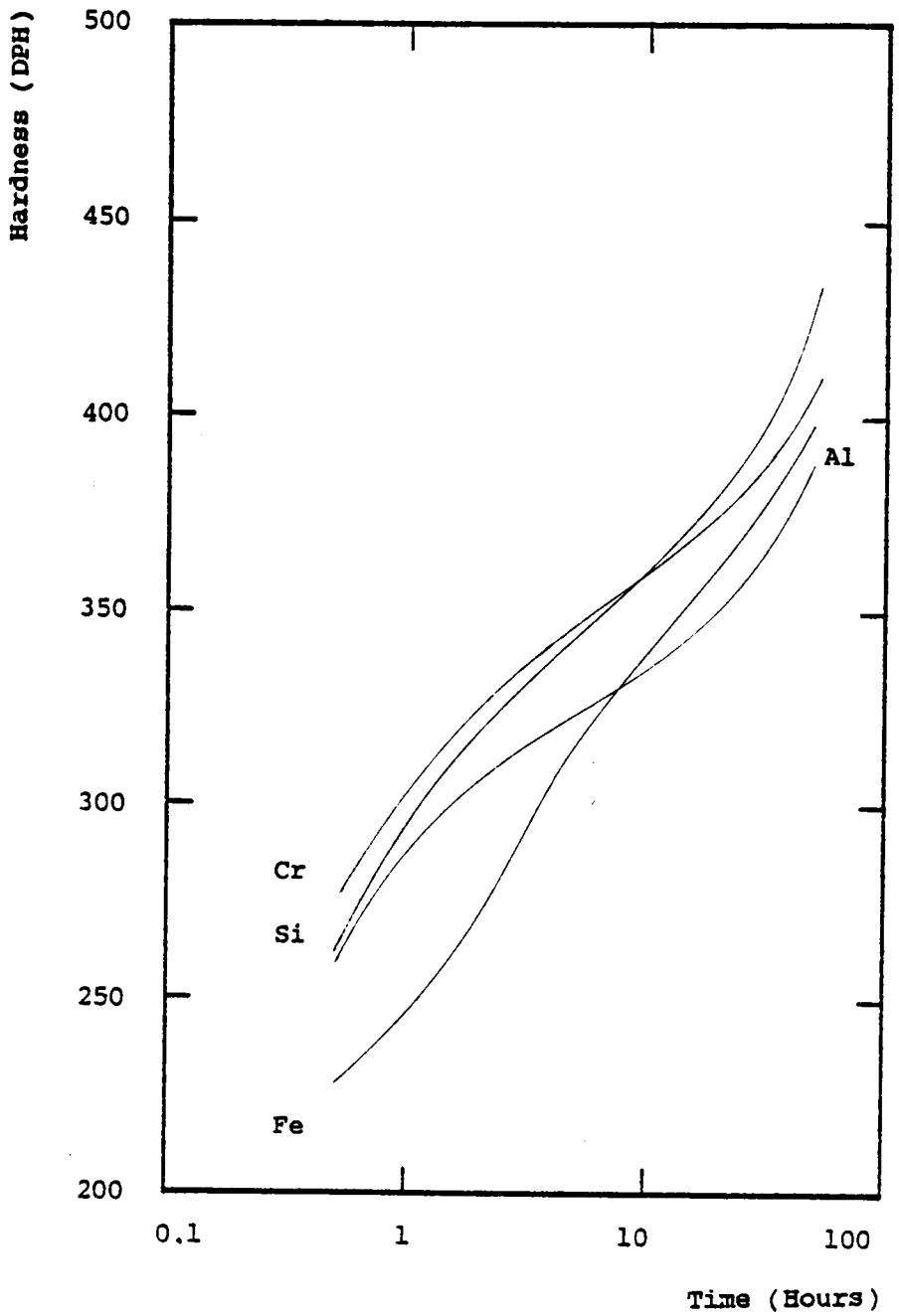


Figure A.15. Hardness of samples with 1 at.% alloy addition, aging temperature 650°C.

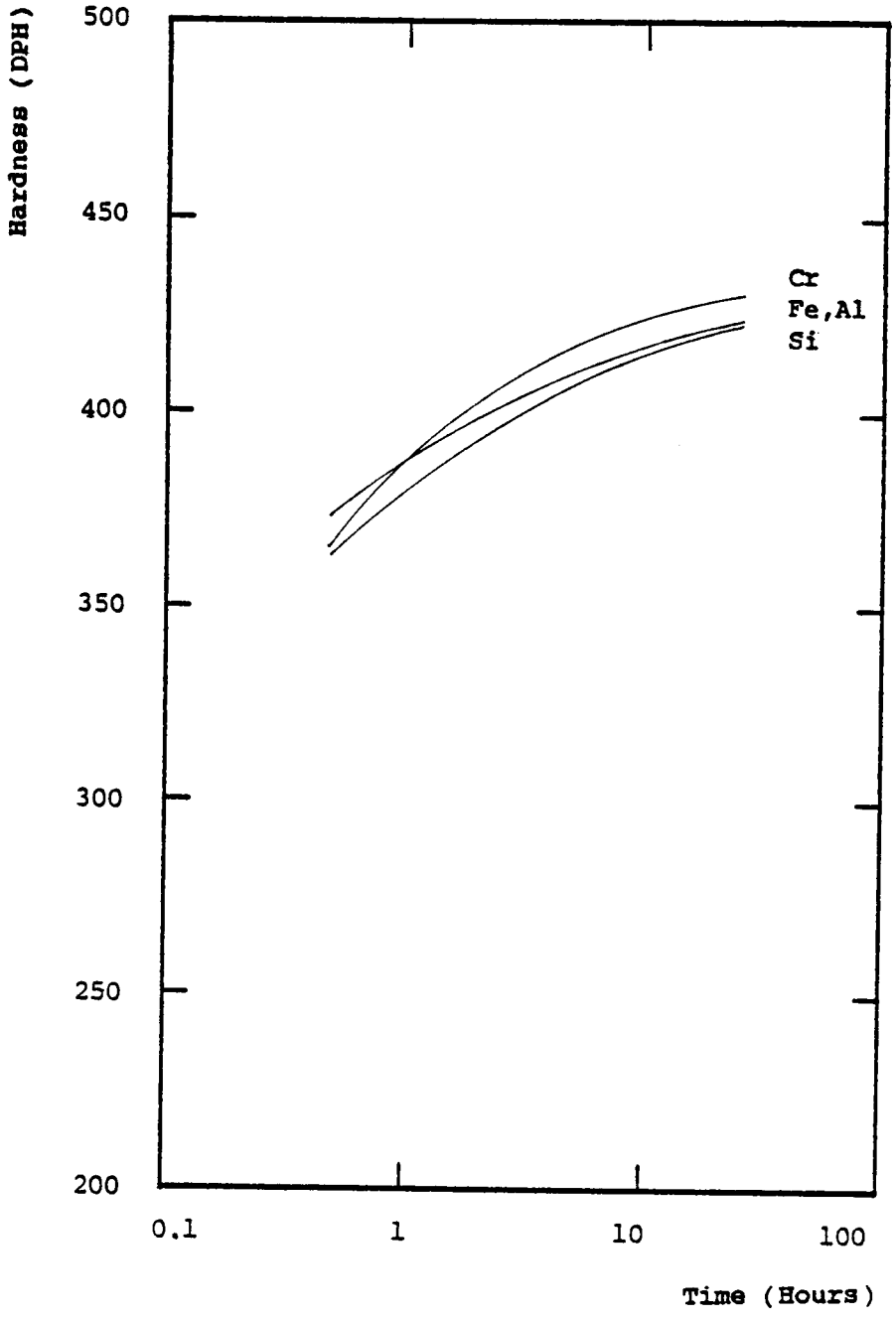


Figure A.16. Hardness of samples with 0.5 at.% alloy addition, aging temperature 750°C.

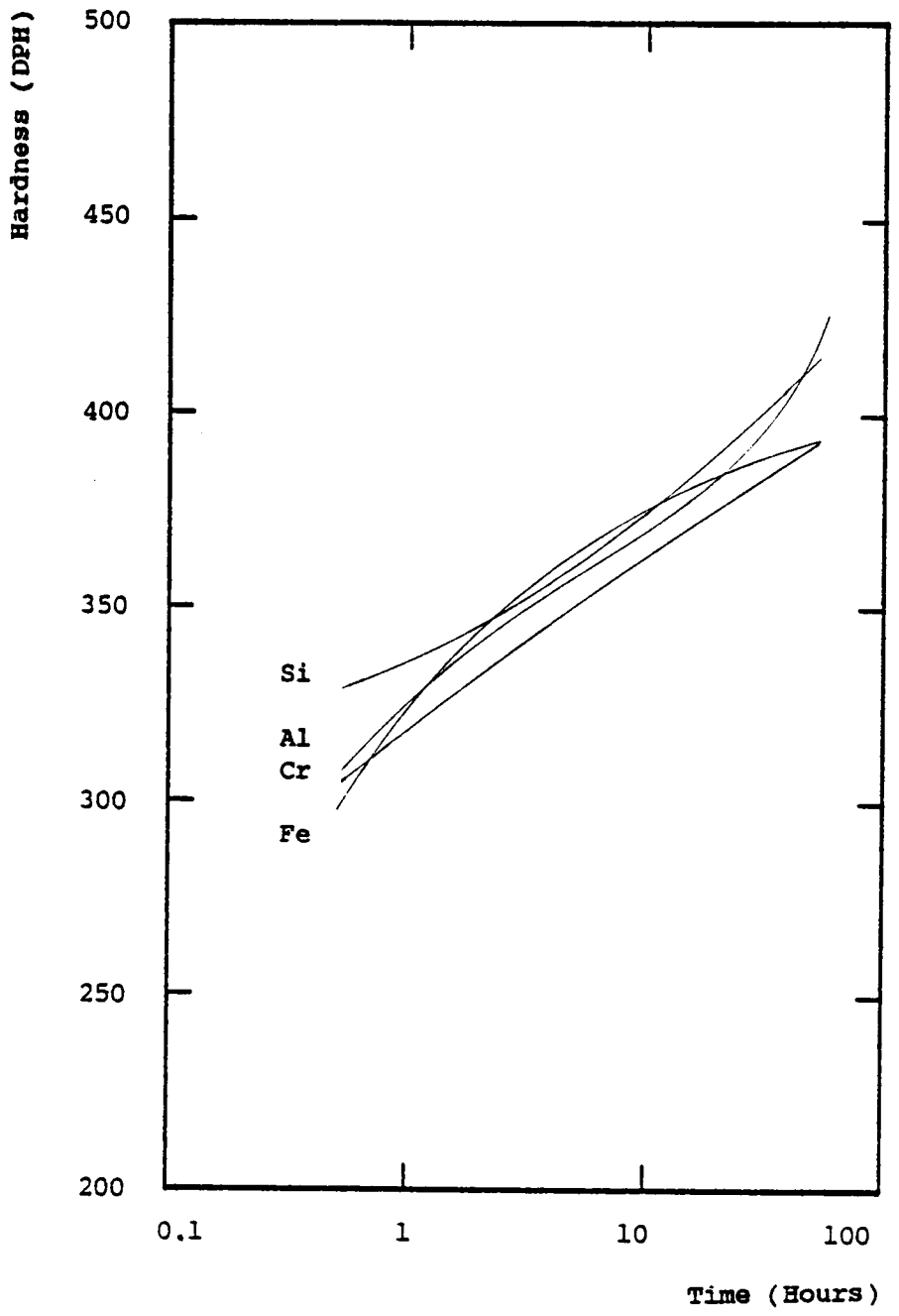


Figure A.17. Hardness of samples with 0.5 at.% alloy addition, aging temperature 700°C.

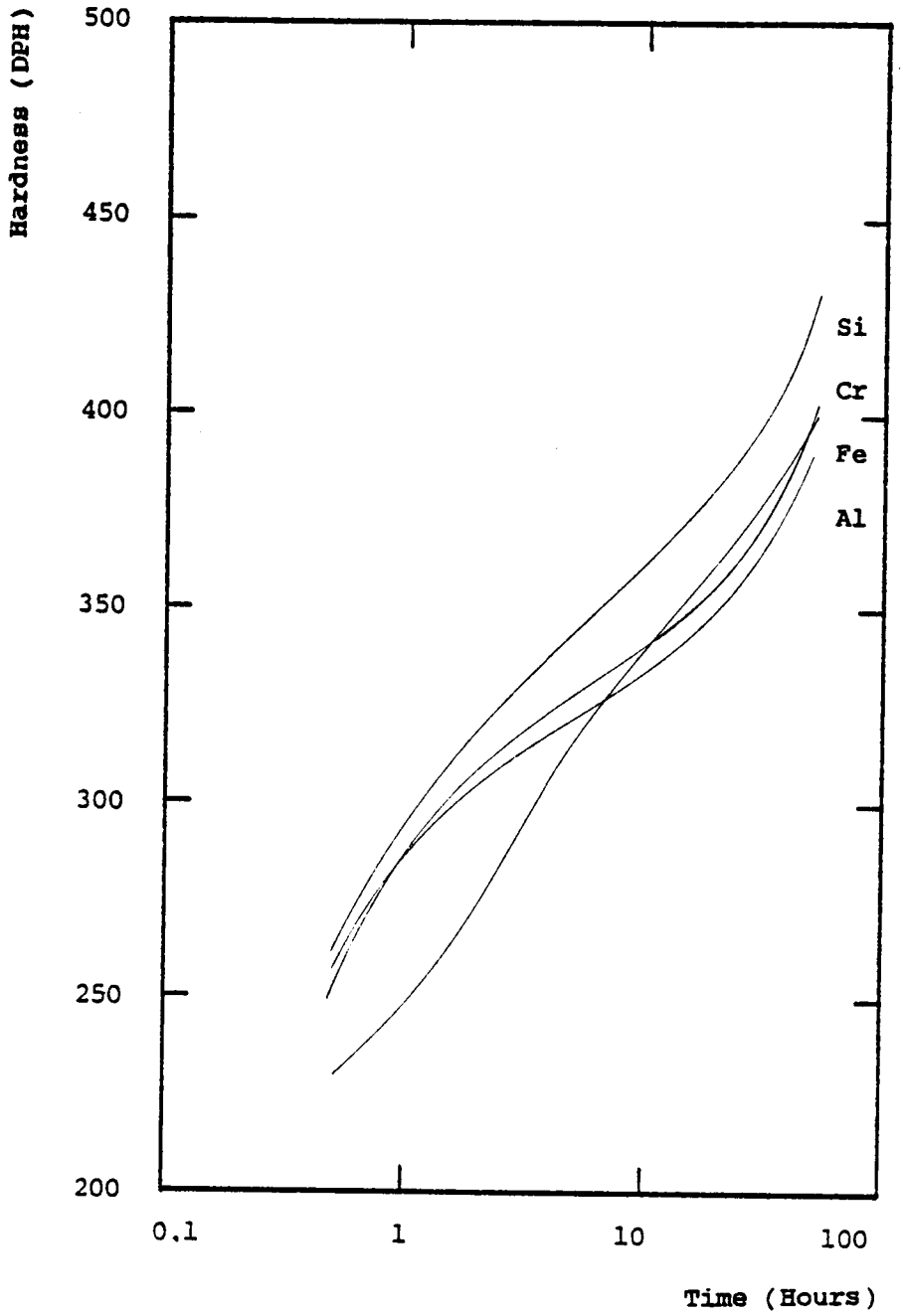


Figure A.18. Hardness of samples with 0.5 at.% alloy addition, aging temperature 650°C.

Table A.1. Integrated intensities after aging 0.5 h. at 650°C.

Alloy	(110)	(101)	(200)	(211)
1% Cr	5390	0	940	330,760
0.5% Cr	2340	0	0	304,790
1% Si	4070	760	550	357,740
0.5% Si	3710	500	450	393,440
1% Fe	6340	730	380	386,920
0.5% Fe	3240	0	570	385,680
1% Al	2720	0	1080	391,240
0.5% Al	3180	320	880	377,700
Ni_4Mo	3500	1000	80	335,380

Table A.2. Integrated intensities after aging 1 h. at 650°C.

Alloy	(110)	(101)	(200)	(211)
1% Cr	570	30	600	180,770
0.5% Cr	2340	220	445	203,000
1% Si	2400	250	630	196,690
0.5% Si	2440	625	225	205,060
1% Fe	2340	290	230	194,540
0.5% Fe	1625	300	635	212,630
1% Al	2030	70	370	194,110
0.5% Al	2010	250	460	213,120
Ni_4Mo	1750	80	80	197,420

Table A.3. Integrated intensities after aging 2 h. at 650°C.

Alloy	(110)	(101)	(200)	(211)
1% Cr	0	100	1130	149,620
0.5% Cr	870	220	1105	191,500
1% Si	1005	210	630	153,810
0.5% Si	190	115	0	195,960
1% Fe	770	330	655	162,210
0.5% Fe	600	140	705	168,710
1% Al	570	405	400	166,860
0.5% Al	1265	680	550	169,760
Ni_4Mo	280	405	585	144,320

Table A.4. Integrated intensities after aging 4 h. at 650°C.

Alloy	(110)	(101)	(200)	(211)
1% Cr	1240	340	450	191,970
0.5% Cr	940	835	555	172,300
1% Si	1140	750	710	174,430
0.5% Si	1465	690	340	192,300
1% Fe	1140	430	400	179,340
0.5% Fe	1450	440	540	195,530
1% Al	860	690	600	185,620
0.5% Al	1590	980	760	191,670
Ni_4Mo	860	970	450	170,390

Table A.5. Integrated intensities after aging 8 h. at 650°C.

Alloy	(110)	(101)	(200)	(211)
1% Cr	920	575	480	168,720
0.5% Cr	760	820	760	163,770
1% Si	730	340	530	161,740
0.5% Si	865	1180	600	182,440
1% Fe	0	230	55	161,290
0.5% Fe	860	180	590	177,120
1% Al	740	845	210	166,080
0.5% Al	1220	880	585	187,790
Ni_4Mo	1095	880	410	161,040

Table A.6. Integrated intensities after aging 24 h. at 650°C.

Alloy	(110)	(101)	(200)	(211)
1% Cr	1060	645	790	152,350
0.5% Cr	615	1305	880	137,540
1% Si	1070	690	955	132,190
0.5% Si	1420	1150	460	157,290
1% Fe	1120	1770	705	164,440
0.5% Fe	960	940	570	144,320
1% Al	1105	770	740	157,950
0.5% Al	1360	1380	500	180,880
Ni_4Mo	1040	1245	990	155,960

Table A.7. Integrated intensities after aging 0.1 h. at 700°C.

Alloy	(110)	(101)	(200)	(211)
1% Cr	220	100	40	210,420
0.5% Cr	770	210	10	213,100
1% Si	570	70	75	195,830
0.5% Si	1330	270	230	191,030
1% Fe	865	105	10	223,920
0.5% Fe	555	570	520	203,140
1% Al	1255	120	320	223,210
0.5% Al	755	95	380	227,460
Ni_4Mo	1030	370	130	231,910

Table A.8. Integrated intensities after aging 0.25 h. at 700°C.

Alloy	(110)	(101)	(200)	(211)
1% Cr	975	690	330	221,580
0.5% Cr	490	510	45	227,790
1% Si	400	740	200	222,240
0.5% Si	340	320	65	196,820
1% Fe	285	130	0	204,740
0.5% Fe	1230	145	2615	220,610
1% Al	80	325	575	222,020
0.5% Al	650	340	120	242,140
Ni_4Mo	540	560	20	250,970

Table A.9. Integrated intensities after aging 0.5 h. at 700°C.

Alloy	(110)	(101)	(200)	(211)
1% Cr	1800	1710	0	222,250
0.5% Cr	1610	1665	50	228,970
1% Si	2730	880	0	226,020
0.5% Si	1510	1040	20	202,910
1% Fe	1710	920	50	217,790
0.5% Fe	1820	940	0	208,170
1% Al	1760	1200	0	224,610
0.5% Al	1755	1405	145	223,900
Ni_4Mo	1500	1530	0	232,300

Table A.10. Integrated intensities after aging 1 h. at 700°C.

Alloy	(110)	(101)	(200)	(211)
1% Cr	2530	2390	0	237,730
0.5% Cr	2330	2515	580	236,980
1% Si	2530	1830	0	225,190
0.5% Si	1980	1810	20	217,090
1% Fe	1930	2160	50	228,070
0.5% Fe	2240	1670	200	221,820
1% Al	2295	1900	0	232,240
0.5% Al	2350	2500	290	223,070
Ni_4Mo	2820	3040	120	246,000

Table A.11. Integrated intensities after aging 2 h. at 700°C.

Alloy	(110)	(101)	(200)	(211)
1% Cr	3705	3170	560	255,220
0.5% Cr	3100	3870	1230	247,150
1% Si	3010	2390	390	239,140
0.5% Si	3105	2850	350	219,520
1% Fe	2720	2660	630	244,550
0.5% Fe	3850	3130	330	229,200
1% Al	2745	2830	460	237,650
0.5% Al	3020	2960	610	233,960
Ni_4Mo	2930	3100	610	242,830

Table A.12. Integrated intensities after aging 4 h. at 700 °C.

Alloy	(110)	(101)	(200)	(211)
1% Cr	4180	3860	1060	229,330
0.5% Cr	4505	5850	905	246,420
1% Si	4230	3390	960	242,090
0.5% Si	4420	3760	1220	225,630
1% Fe	4355	3105	1150	206,510
0.5% Fe	3460	2945	1020	224,160
1% Al	4190	5725	1340	240,030
0.5% Al	4205	4645	1940	236,720
Ni_4Mo	4340	4340	1370	248,040

Table A.13. Integrated intensities after aging 8 h. at 700°C.

Alloy	(110)	(101)	(200)	(211)
1% Cr	4780	4560	1745	234,140
0.5% Cr	4620	4400	1650	246,220
1% Si	5270	4450	2090	251,330
0.5% Si	4460	3600	1470	224,040
1% Fe	4360	3530	1840	228,350
0.5% Fe	4465	3380	2040	227,600
1% Al	3645	4360	1300	229,770
0.5% Al	4670	4745	1670	233,190
Ni_4Mo	5840	5347	2320	247,680

Table A.14. Integrated intensities after aging 24 h. at 700°C.

Alloy	(110)	(101)	(200)	(211)
1% Cr	3760	3450	1570	227,660
0.5% Cr	4260	4610	1770	234,920
1% Si	3700	2780	1345	226,520
0.5% Si	3580	2990	1610	213,650
1% Fe	4090	2740	1240	227,080
0.5% Fe	4470	3370	1775	228,970
1% Al	3550	1100	920	220,190
0.5% Al	4215	4720	1770	234,170
Ni_4Mo	5040	4230	2090	237,000

Table A.15. Integrated intensities after aging 48 h. at 700°C.

Alloy	(110)	(101)	(200)	(211)
1% Cr	3740	4635	1760	227,560
0.5% Cr	4720	4485	1775	231,420
1% Si	3095	2870	1200	224,300
0.5% Si	3590	3580	1480	213,770
1% Fe	3805	3220	1880	222,690
0.5% Fe	3075	2550	920	218,340
1% Al	3530	4050	1520	217,730
0.5% Al	4320	4410	1410	232,515
Ni_4Mo	5200	5095	2410	251,130

Table A.16. Integrated intensities after aging 15 h. at 775°C.

Alloy	(110)	(101)	(200)	(211)
1% Cr	17,555	15,915	8075	443,880
0.5% Cr	15,290	15,650	7160	431,850
1% Si	18,325	15,240	7610	453,730
0.5% Si	16,980	16,650	7390	409,730
1% Fe	7,560	8,870	2700	342,300
0.5% Fe	13,795	13,390	5410	384,130
1% Al	16,420	14,990	6860	437,490
0.5% Al	13,535	13,290	5640	377,230
Ni_4Mo	13,995	14,020	5760	379,800

VITA

Carol P. Fryer was born in Tennessee and attended schools in that state. She received the Bachelor's of Arts degree in French from The University of Tennessee in March 1974, the Bachelor's of Science in Metallurgical Engineering from The University of Tennessee in March 1979, and the Master's of Science in Metallurgical Engineering in March 1982.